Title
Ameloblast Differentiation and Function: Exploring the Effects of microRNA, Fluoride, and Iron

Author
Le, Michael Huan

Publication Date
2016

Peer reviewed|Thesis/dissertation

Ameloblast Differentiation and Function:
Exploring the Effects of microRNA, Fluoride, and Iron

by

Michael Huan Le

DISSERTATION

Submitted in partial satisfaction of the requirements for the degree of

DOCTOR OF PHILOSOPHY

in

Oral and Craniofacial Sciences

in the

GRADUATE DIVISION

of the

UNIVERSITY OF CALIFORNIA, SAN FRANCISCO

[redacted]

Dedication and acknowledgements

This project would not have been possible without the mentorship of my advisor, Dr. Pamela Den Besten, who has provided me with significant advice, feedback, and wisdom in the scientist portion of my clinician scientist training. I have been able to do many things that I would have otherwise thought I was not capable of doing during my PhD training at UCSF.

I would also like to thank Dr. Yukiko Nakano, whose guidance in laboratory techniques, data analysis, subject matter expertise, and limitless patience were crucial to obtaining the results I report in this dissertation.

I would also like to thank Drs. Li Zhu, and Yan Zhang, and all those I worked with in the Den Besten laboratory for their support and encouragement over the past five years.

I would also like to thank Drs. Wu Li, Noelle L'Etoile, and Stefan Habelitz for being a part of my dissertation committee, providing an additional source of insight, encouragement, and support.

I would also like to thank my present and past peers in the both Oral and Craniofacial Sciences PhD program who have provided me with numerous opportunities to take a (brief) break from research and enjoy the many of little things that life offers daily, while making many incredible memories in the process.

I would also like to thank the students who make up the UCSF School of Dentistry during my time as a PhD student at UCSF. They have welcomed me to be a part of their class, not only allowing me to stay engaged in clinical dentistry and provide opportunities to share my clinical wisdom during my PhD training, but also helping me maintain the clinician aspect of being a clinician scientist.

Lastly, I would like to thank my family for their patience and understanding in this path I have taken, as I have been much too busy to talk and see them as often as they like during these past nine years. And my girlfriend, Cynthia, who has never ceased to be my greatest supporter these past ten years, especially in the last five years as we simultaneously underwent the trials, tribulations, and triumphs in earning a PhD in the biological sciences.

Abstract

During amelogenesis (dental enamel formation), ameloblast cells undergo several morphological and functional changes as they form dental enamel. Interference in the timing of these changes results in enamel of poor quality, affecting the psychosocial development of children at a crucial age of their development. However, the mechanisms that facilitate these transitions in ameloblasts are not well understood. Using rodent models as a basis for study, I used microRNA, fluoride, and iron as tools to carry out histological, immunochemical, and quantitative PCR experiments that investigate the mechanisms that regulate and define ameloblast differentiation and function.

As ameloblasts differentiate from one phase to another during amelogenesis, many genes are simultaneously up- and down- regulated. MicroRNAs serve as one mechanism for rapid control of post-transcriptional expression of many genes. Amelogenin, the predominant protein found in the enamel matrix, is alternatively spiced and may serve as a source for microRNAs. I found that exon 4 of the amelogenin gene produces a microRNA that regulates expression of Runx2, a key transcription factor for when ameloblasts are secreting the enamel matrix.

Ameloblasts express and secrete KLK4, a crucial enzyme that facilitates the final phase of amelogenesis. However, it is unclear how ameloblasts begin increasing *Klk4* expression at the right time. I found that androgen receptor (AR) serves as an intracellular regulator of expression for *Klk4* and that exposure to fluoride inhibits AR translocation to result in decreased *Klk4* expression and synthesis.

Normal rodent ameloblasts deposit iron onto the enamel surface, resulting in yellow-brown colored surface enamel. This pigment is lost in rodents sensitive to high levels of fluoride. Iron in the surface enamel is thought to increase wear resistance in the enamel, though it is unclear how ameloblasts acquire, manage, and transport iron for deposition into enamel. I found that fluoride exposure resulted in a significantly increased expression of ferroportin (iron-exporting protein), and significantly decreased expression of the heavy chain subunit of ferritin, which facilitates the safe storage of iron in cells.

Furthermore, it appears that changes in these iron-related proteins by fluoride may be changing free intracellular iron levels to affect expression and synthesis of oxidative stress-related genes.

These studies have shown that multiple mechanisms are responsible for ameloblast differentiation. The effects of fluoride on ameloblast differentiation appear to be largely due to cellular effects of fluoride rather than fluoride related changes in the enamel matrix.

Table of Contents

Chapter 1 – Introduction 1

Chapter 2 – Amelogenin Directs Ameloblast Differentiation 6

Chapter 3 – Fluoride Downregulates Klk4 Expression Through Inhibition of Androgen Receptor Activation 21

Chapter 4 – Tracing Iron Transport Through Ameloblasts in Rodent Incisor Pigmentation 34

Chapter 5 – Summary and Future Directions 47

References 49

Appendix 1 – The Complex Regulation of Klk4 Expression by TGF-β and Androgen Receptor Signaling in Amelogenesis 55

Appendix 2 – Genetic Influences on Fluoride's Effect on Ameloblast Differentiation 64

Appendix 3 – Primers sequences used for all qPCR experiments 74

List of Tables

Table 1: Primers sequences used for all qPCR experiments 74

List of Figures

Figure 1: Prediction of amelogenin exon4 miRNA 9

Figure 2: miRNA derived from exon4 (miR-exon4) is generated from amelogenin 10

Figure 3: miR-exon4 is present in the mouse enamel organ 11

Figure 4: Expression of major splicing variants of amelogenin mRNAs without exon4 (LF-4 and SF-4) and its exon4 included variants 11

Figure 5: miR-exon4 was present in mouse developing enamel organ 12

Figure 6: Runx2 expression was up-regulated by miR-exon4 mimic in LS8 cells 13

Figure 7: miRNA derived from exon4 (miR-exon4) is expressed in Amel knockout (KO) enamel organ 14

Figure 8: Ameloblasts from amel knockout (KO) mice are similar to WT mice 15

Figure 9: Expression of Runx2 is downregulated in Amel knockout (KO) enamel organ at the secretory stage (P5) 16

Figure 10: Downstream targets of Runx2 were downregulated in Amel KO enamel organ 17

Figure 11: Alignment of intron7 vs. exon4 and intron4 in mouse amelogenin gene (gene ID 11704) 19

Figure 12: Fluoride decreased in vivo KLK4 activity and Klk4 expression 26

Figure 13: Ar^{Tfm} mice exhibit enamel matrix protein retention similar to fluoride exposed mice 27

Figure 14: Fluoride altered expression CCND1 and TGFBR2, regulators of androgen receptor activation 28

Figure 15: Fluoride does not alter *Klk4* or *Ar* expression at near physiologic serum fluoride levels 29

Figure 16: Fluoride significantly upregulated ferroportin (*Fpn*) expression without affecting expression or synthesis of transferrin receptor (*Tfrc*) 38

Figure 17: Fluoride did not affect ferric iron levels in maturation ameloblasts 39

Figure 18: Fluoride significantly affected expression of the heavy chain subunit of ferritin (*Fth*) 40

Figure 19: Fluoride increased activation of NFκB and decreased SOD1 synthesis in maturation ameloblasts 41

Figure A1: 129/SvImJ mice do not exhibit matrix retention when exposed to fluoride 58

Figure A2: Fluoride reduced androgen receptor translocation in 129 mice 59

Figure A3: While fluoride reduced TGFBR2 synthesis like in C57,
it increased TGFB1 synthesis in 129 mice 60

Figure A4: Male C57 mice have significantly reduced AR translocation, intermediate between
female mice and ArTfm where AR, though reduced, still translocated 61

Figure A5: Fluoride can induce maturation ameloblasts to have an
early shortening morphology in C57BL/6 mice 67

Figure A6: Detection of iron and heavy chain ferritin (FTH) synthesis correlates with
maturation ameloblast layer length 68

Figure A7: 129/SvImJ can exhibit a shortened maturation ameloblast layer when exposed to fluoride 69

Figure A8: Exposure to 50 ppm F did not affect incisor pigmentation in 129/SvImJ mice 70

Figure A9: Distribution of lengths of individual mice when exposed to 0 or 50 ppm F 71

Figure A10: Quantitative polymerase chain reaction strategy to quantify
the expression of amelogenin mRNA splice variants 76

Chapter 1
Introduction

Dental enamel is the highly mineralized protective outer covering of teeth, conferring strength, abrasion resistance, and protection of the teeth in the oral cavity (Shimizu and Macho, 2008). The formation of dental enamel, called amelogenesis, occurs in two main stages (Hu et al., 2007). In the first, or secretory, stage, an enamel matrix (composed of mainly amelogenin proteins) is secreted to support elongating enamel crystals. The crystals grow with select hydrolysis of matrix proteins by matrix metalloproteinase 20 (MMP20). When the enamel crystals reach their final length, the maturation, stage begins. In the maturation stage, the enamel matrix is hydrolyzed by kallikrein-related peptidase 4 (KLK4) to create room for the widening enamel crystals.

In mammals, amelogenesis is directed by the cells of the enamel organ. Within the enamel organ, the ameloblasts, which directly overlay the enamel matrix, have a specific morphology and function depending on the stage amelogenesis (Hu et al., 2007). Secretory ameloblasts are highly polarized, columnar, and form a unique cellular extension called a Tomes' process by which enamel matrix proteins are secreted to form the enamel matrix. Proteolytic enzymes like MMP20 are simultaneously secreted through Tomes' process to rapidly hydrolyze the enamel matrix to facilitate the elongation of the hydroxyapatite crystals. When secretory ameloblasts differentiate (or transition) into maturation ameloblasts, they then become cuboidal in shape. At this stage, the ameloblasts modulate between ruffle and smooth bordered cells and secrete proteinases including KLK4 to further hydrolyze the enamel matrix proteins, allowing space for mineral apposition at the sides of the crystals to expand their width.

The mechanisms regulating ameloblast differentiation are not well understood. It is unclear how ameloblasts initiate their initial function of secreting an enamel matrix, then rapidly switch function to one that promotes the rapid degradation and mineralization of that enamel matrix (Hu et al., 2007). In the transition from secretory to maturation stage, genes predominantly expressed in secretory ameloblasts such as amelogenin (*Amel*), the predominant protein of the enamel matrix, and *Mmp20* are quickly

downregulated in favor of genes predominantly expressed primarily in maturation ameloblasts such as *Klk4*, amelotin (*Amtn*), and odontogenic ameloblast-associated protein (*Odam*).

The hallmark of secretory stage amelogenesis is the upregulation of expression of amelogenins. Amelogenins are alternatively spliced proteins that are expressed in large quantities and are know to promote the elongation of enamel matrix crystals in the enamel matrix. Altering expression of any one of the at least 17 known alternative spliced amelogenin transcripts will affect ameloblast differentiation (Simmer et al., 1994; Stahl et al., 2013). Interestingly, many *Amel* transcripts often lack inclusion exon 4 of *Amel*, and the two major isoforms of AMEL do not include any peptides encoded by exon 4.

One type of widespread control of post-transcriptional expression of many genes simultaneously is one mediated by micro RNAs (miRNA), which are a small non-coding RNA molecules containing about 22 nucleotides (Bartel, 2009). In ameloblasts, different miRNAs are known to be differentially expressed between secretory and maturation stage ameloblasts (Yin et al., 2014), and contribute to ameloblast differentiation (Michon et al., 2010). For example, altered expression of microRNA 224 in ameloblasts result in enamel with reduced hardness due to disrupted organization of the enamel crystals (Fan et al., 2015). However, it is unknown if any microRNAs specifically regulate the differentiation ameloblasts.

While some miRNAs are their own non-protein coding gene, others will derive from the introns or exons of protein-coding genes (Kim et al., 2009). This suggests certain miRNAs could form from the products of alternative splicing events. Furthermore, ectopic expression of exon 4 results in enamel being hypomineralized due to disruption of secretory ameloblasts (Cho et al., 2014). Thus, if exon 4 is often skipped during amelogenesis, why does exon 4 exist? Could it be a source of miRNA to regulate ameloblast function?

Yet, miRNA is not the only type of molecule that affects ameloblast function during amelogenesis. Excessive exposure to fluoride (F) during amelogenesis results in dental enamel fluorosis. The severity of fluorosis depends on the duration and dosage of fluoride exposure (Denbesten and Li, 2011). While

exposure to 1 ppm F may result in enamel developing white streaks in some individuals, others exposed to higher levels (5 ppm or more) will often have enamel that is mottled and mechanically weak. This mechanical weakness is a result of retained protein in the enamel matrix (Den Besten, 1986). Yet, it is unclear how fluoride exposure results in retained protein in the dental enamel. One hypothesis is that fluoride decreases expression of *Klk4* through changes in transforming growth factor-β (TGF- β) signaling (Suzuki et al., 2014). With decreased *Klk4* expression, there would be less KLK4 protein to degrade the enamel matrix, perhaps making it difficult for maturation ameloblasts to resorb the enamel matrix to complete enamel mineralization.

Another hypothesis that has been developed centers on the ability of maturation ameloblasts to manage the pH of the enamel matrix. The enamel matrix acidifies as a result of hydroxyapatite biomineral (HAP) formation, $10\ Ca^{2+} + 6\ HPO_4^{2-} + 2\ H_2O \rightarrow Ca_{10}(PO_4)_6(OH)_2 + 8H^+$, producing protons that acidify the enamel matrix. During maturation stage amelogenesis, there is increased enamel HAP mineralization compared to secretory stage, producing more protons that are neutralized through the action of various ion exchangers that maintain the enamel matrix pH between an acidic 5.6 and a neutral 7.2 (Jalali et al., 2014; Lyaruu et al., 2008; Sasaki et al., 1991). These pH modulations in the enamel matrix correlate with morphological modulations seen with maturation ameloblasts. Changing the pH regulatory system through retention of amelogenin in the enamel matrix or reducing concentration of certain ions such as chloride (Bronckers et al., 2015), which is found in the presence of fluoride during amelogenesis, is known to affect the rate of morphological modulations in maturation ameloblasts (DenBesten et al., 1985; Smith et al., 1993).

Because of the dynamic interaction between ameloblasts and the enamel matrix during amelogenesis, it is unclear if any observed cellular changes in maturation ameloblasts are due to direct changes by fluoride, or merely a byproduct of fluorotic changes to the enamel matrix. For example, studies in rodents given 50 ppm F showed incomplete hydrolysis and removal of the enamel matrix proteins (Den Besten, 1986).

Thus, is the incomplete hydrolysis of enamel matrix proteins in fluorosed enamel, due to fluorotic changes to the enamel matrix, or fluoride changes ameloblasts to produce less proteolytic enzymes? There is evidence that fluoride has specific cellular effects, such as altered gene expression profiles in ameloblasts overlying fluorosed enamel as compared to controls through fluoride-related increase of $G_{\alpha q}$ activity in secretory ameloblasts (Zhang et al., 2014), suggesting the possibility that fluoride directly alters gene expression, though this is yet to be determined *in vivo*. Nonetheless, fluoride can serve as a tool to explore the signaling mechanisms responsible for ameloblast differentiation and function.

Studies to determine how fluoride affects amelogenesis rely on rodent models as it is not possible to do similar studies using human teeth. An added benefit of using rodent models is their continuously growing incisors, which allow the effects of fluoride to be seen at all stages of amelogenesis. Although fluoride can be given in drinking water beginning when rodents are 21 days old (the time when rodents are weaned), rodents need to be exposed to approximately 10 times the amount to result in the same serum fluoride levels seen in humans (Den Besten, 1986; Guy W et al., 1976). For example, For example, humans drinking 3-5 ppm fluoride in water (1 ppm F = 52.6 µM) have serum fluoride levels of 3-5 µM (Guy W et al., 1976), resulting in fluorosed enamel. For a mouse to have similar serum fluoride levels, the mouse must ingest drinking water containing approximately 50 ppm F (Zhang et al., 2014). Because of the dramatic difference in levels of ingested fluoride to result in similar serum fluoride levels in humans and rodents, there has been confusion on the relevance of *in vivo* and *in vitro* studies of fluoride mechanisms.

Yet, using rodent models to study the effects of fluoride on amelogenesis also has an additional side effect, as rodents exposed to excessive amounts of fluoride also have reduced incisor pigmentation (Everett et al., 2002). This pigmentation is iron based, as rodents on iron-deficient diets have reduced pigmentation in their incisor (Halse, 1973), negatively impacting the acid resistance and hardness characteristics of the enamel (Berkovitz and Heap, 1976; Dumont et al., 2014). This iron-based pigment appears to be deposited on the surface enamel by mid- to late- maturation ameloblasts (Wen and Paine, 2013), and only appears as the enamel reaches its mature mineral content (Halse, 1972a; Halse and

Selvig, 1974). In cases of severe iron deficiency, the enamel is hypoplastic due to a disturbed arrangement of crystals and the ameloblasts have less pigment and organization (Prime et al., 1984). Furthermore, while human enamel is not pigmented as seen in rodents, several studies have noted an association between anemia and increased incidence of severe early childhood caries in humans (Bansal et al., 2016; Schroth et al., 2013; Tang et al., 2013). These studies taken together suggest that iron plays an important, but not very well understood, role in amelogenesis.

Interestingly, during amelogenesis, it is unclear why iron accumulates only in maturation ameloblasts. Iron accumulation is often associated in situations when cells are experiencing oxidative stress, as excessive intracellular levels of free iron promote increased formation of reactive oxygen species (ROS) (Kruszewski, 2003). Excessive amounts of ROS result in altered cellular function due to increased damage to biomolecules like DNA and proteins (Sheng et al., 2013). However, if a majority of the accumulated iron found in cells is bound to protein, then iron accumulation instead confers protective effects to the cell by reducing a source for ROS formation (Sturrock et al., 1990), and a few *in vitro* studies have shown that exposing cells to millimolar levels of fluoride induces oxidative stress (Liu et al., 2011; Shuhua et al., 2012). Thus, it is unclear how fluoride-induced reduced pigmentation occurs, as it could be a result of ameloblast responding to oxidative stress by increasing retention of iron (resulting in lack of pigmentation) or due to the hypomineralized characteristic of fluorotic dental enamel.

Therefore, this dissertation aims to explore the various mechanisms that regulate ameloblast differentiation and function. To address this question, I have investigated the possibilities that transcription of amelogenin gene directly contributes to the formation miRNA derived from exon 4 to regulate secretory ameloblast function (Chapter 2); fluoride can directly alter KLK4 expression and synthesis (Chapter 3); and that fluoride may iron accumulation in maturation ameloblasts during amelogenesis (Chapter 4). These studies have led me to an appreciation of the delicate interplay between cells and the extracellular matrix in amelogenesis, and the challenges in determining elucidating interplay needed between the two to result in amelogenesis that produces high quality enamel.

Chapter 2
Amelogenin Directs Ameloblast Differentiation

2.1 Introduction

Ameloblast differentiation can be effected by altering expression of any one of the 17 amelogenin transcripts during amelogenesis (Simmer et al., 1994). Many amelogenin isoforms typically lack exon 4, including the major variants that include exon 6abc, or have exon 6abc skipped (Ye et al., 2006). Forcibly expressing amelogenin transcripts that contain exon4 during amelogenesis result in enamel being hypomineralized due to disruption of secretory ameloblasts (Cho et al., 2014). Furthermore, immuno-localization of amelogenin proteins containing exon4-coded peptide shows them to be present in early maturation-stage enamel matrix (Stahl et al., 2015). These findings suggest the proper exclusion and inclusion of exon4 in amelogenin splice variants may correlate with ameloblast differentiation and is strictly regulated during amelogenesis.

Examination of the sequence of amelogenin exon4, we found potential properties of a mature miRNA (miR-exon4) contained within the exon sequence. Mature miRNA are a class of naturally occurring and small non-coding single-stranded RNA consisting of 18-24 nucleotides that can bind to target mRNAs to modulate protein synthesis resulting in altered development, apoptosis, and cell cycle regulation (Bartel, 2004) including tooth development (Michon et al., 2010). Mammalian miRNA loci reside in introns or exons of their pre-mRNA host genes, sharing the regulatory elements, or exist as separate genes transcribed from their own promoters (Kim et al., 2009). Among miRNAs, an exonic miRNA is created by the host gene's alternative splicing or through transcription by an independent promoter (Marsico et al., 2013).

Using Amelogenin KO and WT mice, I will explore the role of miR-exon4 during ameloblast differentiation.

2.2 Materials and Methods

Animals

A mixed background (C57BL/6J x SJL) WT mice and *Amel* KO and WT mice (a kind gift from Dr. Carolyn Gibson, University of Pennsylvania) (Gibson et al., 2001a) colonies were maintained at University of California-San Francisco (UCSF) animal facility. The animal handling protocol was approved by the UCSF animal care committee. At postnatal day 0 (P0), 5 (P5) and 10 (P10), mice were euthanized and developing first molars (Nakano et al., 2004) were harvested and processed for miRNA and RNA extraction.

Extraction of RNA and miRNA

Total miRNA and mRNA was purified molar tooth organs using the miRNeasy and RNeasy MinElute Cleanup Kits (Qiagen, Germantown, MD). The tooth organs were not homogenized so that miRNA and mRNA would be primarily extracted from the exposed enamel organs overlying the tooth organ. For selective conversion of mature miRNA into cDNA, reverse transcription was performed using miSript II RT kit (Qiagen). cDNA was obtained by reverse transcription of the mRNA using Superscript III First-Strand Synthesis Supermix for qRT-PCR (Life Technologies).

qPCR analysis

Expression of miRNA was characterized by qPCR with the miScript SYBR Green PCR Kit and a custom made primer for miR-exon4 (Qiagen), using the ABI 7500 system (Applied Biosystems, Foster City, CA). Hs_RNU6-2 was used as a reference gene. Expression of mRNAs was examined by qPCR with FastStart Universal SYBR Green Master kit (Roche Diagnostics, Indianapolis, IN) using primer sets for Amel (exon6b-d), Ambn, Enam, Mmp20, Runx2, Tgfbr2, Wnt10b, Odam, and Amtn (Elim Biopharmaceuticals, Hayward, CA). MRPL19 was used as a reference gene. For amplification of a long amplicon with a primer set for Amel (exon4-6d), a KOD SYBR® qPCR Mix (Toyobo, Osaka, Japan) was used (primer sequences are listed in Appendix 3). Expression of amelogenin mRNA splice variants, including amelogenins containing exon6abc (long form with or without exon4, LF+/-4), and amelogenins

lacking exon6abc (short form with or without exon4, SF+/-4) were quantified by primer sets and Taqman probes (Elim Biopharmaceuticals) (Appendix Figure A10) using FastStart TaqMan® Probe Master kit (Roche Diagnostics).

Histology

At postnatal days of 21, mice were euthanized and mandibles were dissected out for immersion fixation in 4% paraformaldehyde in 0.06M Na-cacodylate buffer (pH 7.3) at 4 °C for 24 hours. After decalcification in 8% EDTA (pH7.3), samples were processed for routine paraffin embedding and sectioning. Deparaffinized sections were stained with H&E staining.

2.3 Results

miR-exon4 was produced from the amelogenin gene

Our analysis of the exon4 sequence showed characteristics of a primary miRNA. These features of the exon4 mRNA sequence included: (1) it is short (52 nt) with a possible hairpin secondary structure (modeled with Vienna RNA version2.0) (Lorenz et al., 2011), (2) it has a sequence with 57th percentile score homology to a known miRNA (hsa-miR-3660, which resides in non-protein coding gene on chromosome 5), (3) it has a primary miRNA recognition site (splicing factor SRSF3 binding motif CNNC) downstream (16-18 nt) from the predicted mature miRNA motif (Auyeung et al., 2013) (Fig 1).

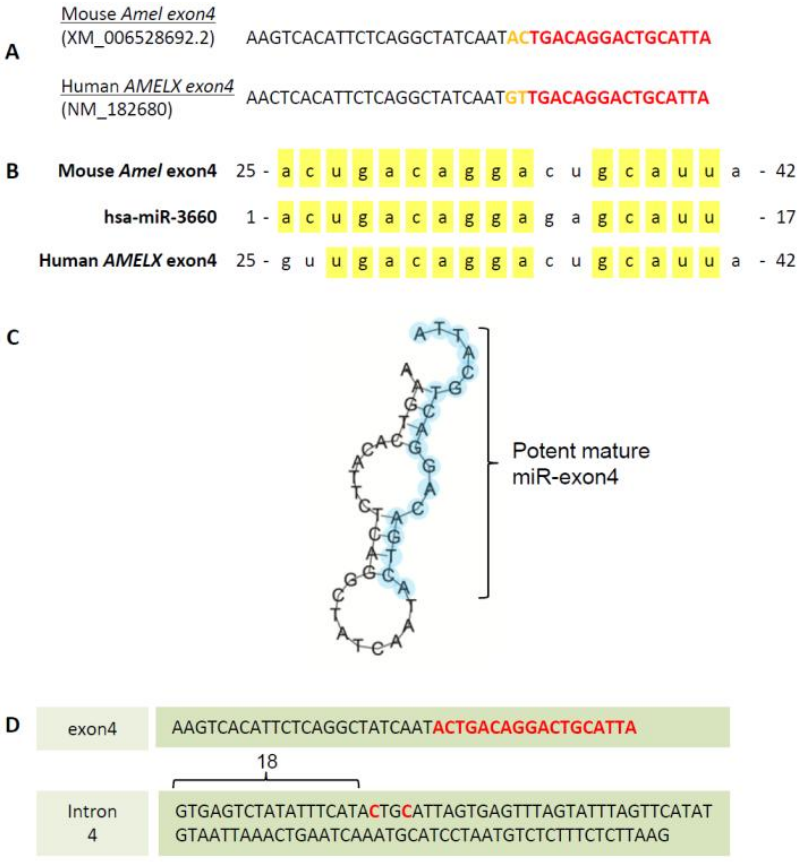

Figure 1 *Prediction of amelogenin exon4 miRNA*
(A) cDNA sequence of mouse and human amelogenin exon4 is highly conserved. Putative miRNA sequence is in red. B) Sequence homology between amelogenin exon4 mRNA (mouse and human) and hsa-miR-3660. Homologous sequences are highlighted in yellow. C) Secondary structure of mouse exon4 RNA predicted at The Vienna RNA website. Potent mature miR-exon4 sequence is highlighted in blue. D) Presence of CNNC sequence at 18+1 nucleotide downstream from the putative miRNA (in red) in mouse amelogenin cDNA sequence (XM_006528692.2).

To determine whether this potential mature miRNA derived from exon4 (miR-exon4) is generated from the amelogenin gene, we transfected an amelogenin minigene, which contained the translated region of mouse *Amel* (exons 2-7 and introns 2-6) into LS8 cells. Expression of miR-exon4 was identified by qPCR, and was greatly upregulated after amelogenin minigene transfection (Figure 2). To further confirm that the mature miR-exon4 was derived from the amelogenin minigene, we introduced a C to T mutation (C.144+19C>T) at the potential primary miRNA recognition site at the predicted miRNA stem base (CNNC motif) (Auyeung et al., 2013) in the amelogenin minigene, located 18+1 nt downstream the putative mature miR-exon4 sequences. The mutated amelogenin minigene produced significantly reduced amount of mature miR-exon4 (Figure 2).

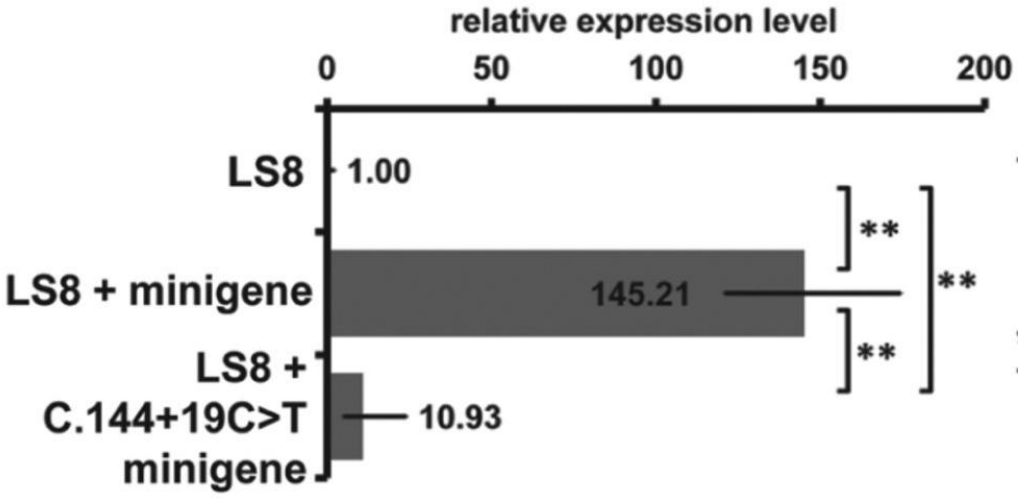

Figure 2 *miRNA derived from exon4 (miR-exon4) is generated from amelogenin*
Transfection of the cells with an amelogenin minigene greatly increases (145 times of control) the production of miR-exon4 in LS8 cells. Mutation of the CNNC sequence (C.144+19C>T) significantly reduces the miR-exon4 in cells transfected with the amelogenin minigene. Expression levels are demonstrated as the relative expression level (fold change) compared with control (LS8 cells without transfection). Each bar represents a 95% confidence interval. The significance of differences between control and test values was determined by the *t* test with Bonferroni correction following 1-way analysis of variance (3 comparisons in 3 groups). $^{**}P < 0.01$, $n = 3$ in each group.

80% of exon4 was spliced and available for miRNA processing

In mouse, as well as human, most of amelogenin mRNA variants including the major splice variants are known to lack exon4. This indicates that exon4 is mostly available for miRNA processing, although the exact availability is not known. To determine the proportion of exon4 available for miRNA processing, we used qPCR to quantify the relative amounts of amelogenin without exon4, compared with amelogenin with exon4, at presecretory (P0), secretory (P5) and maturation (P10) stages of enamel formation in the mouse enamel organs. These analyses showed that most of the amelogenin mRNAs were without exon4 at all stages (P0: 88.54%, P5: 89.26% and P10: 73.03%) indicating that around 80% of exon4 was spliced out throughout ameloblast differentiation (Fig 3). All splice variants were most highly expressed at P5/secretory stage when the peak expression of amelogenins was observed (Fig 4).

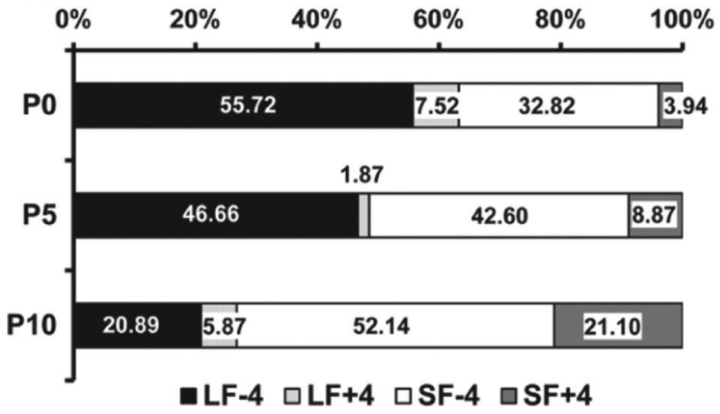

Figure 3 *miR-exon4 is present in the mouse enamel organ*
Expression of major splicing variants of amelogenin mRNAs without exon4 (LF-4 and SF-4) and their exon4-included variants (LF+4 and SF+4) are demonstrated as percentages of total amelogenin mRNA per stage. At any stage, variants without exon4 (LF-4 and SF-4) are present in greatest quantity (73.03% to 89.26%) of detecting amelogenins (n = 4).

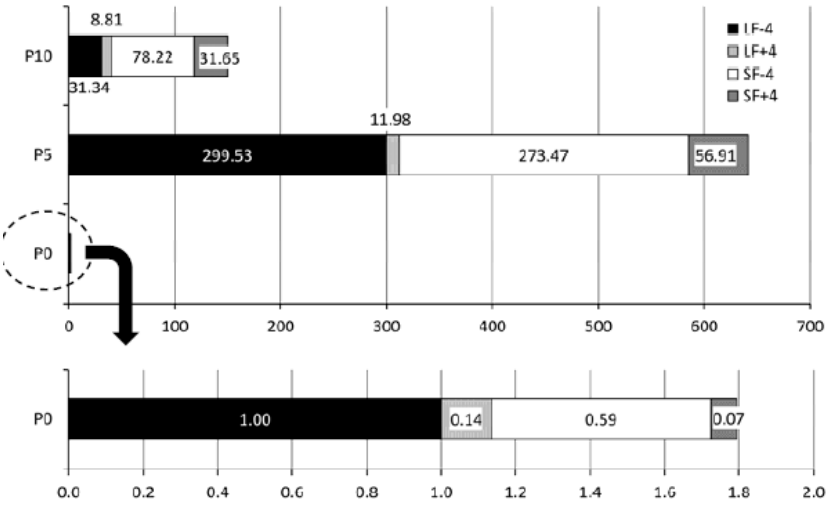

Figure 4
Expression of major splicing variants of amelogenin mRNAs without exon4 (LF-4 and SF-4) and its exon4 included variants (LF+4 and SF+4) was quantified as the relative expression level (fold change) compared with expression level of LF-4 at P0/pre-secretory stage as 1. All four variants reached the highest expression level at P5/secretory stage resulting in peak of overall amelogenin expression at this stage. n=4

miR-exon4 was present in mouse developing enamel organ

To determine the presence of mature miR-exon4 in vivo, we examined the expression of miR-exon4 in WT (C57BL/6J x SJL) mouse enamel organ at presecretory (P0), secretory (P5) and early maturation (P10) stages by qPCR. The mature miR-exon4 was amplified at all developmental stages, with highest expression in P5/secretory enamel organ, and decreasing in P10/early maturation enamel organ (Fig 5).

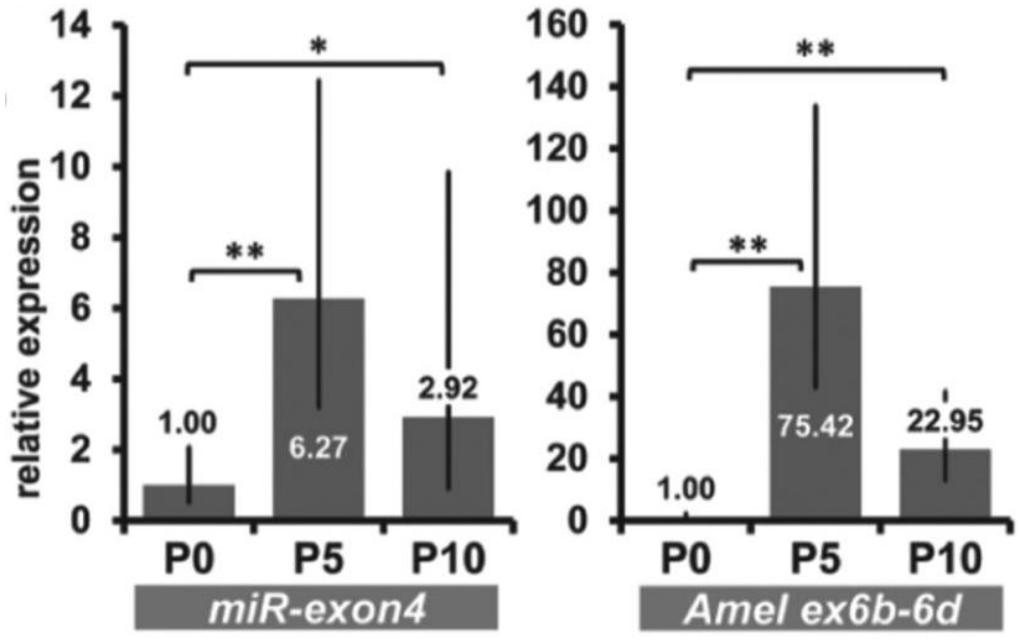

Figure 5 *miR-exon4 was present in mouse developing enamel organ to upregulate important amelogenesis genes* miR-exon4 is expressed in C57BL/6J x SJL mixed mouse enamel organ at all presecretory (P0), secretory (P5), and early maturation (P10) enamel organs (left panel). Expression profile of miR-exon4 is similar to those of LF amelogenin (include exon6b-6d) mRNA (right panel). Expression of mRNAs is demonstrated as the relative expression (fold change) level compared with P0 WT. Each bar represents a 95% confidence interval. The significance of differences between P0 and P5 or P10 values was determined by the 2-tailed multiple *t* test with Bonferroni correction following 1-way analysis of variance (3 comparisons in 3 groups). **P* < 0.05, ***P* < 0.01, *n* = 5 in each group. P0, P5, P10: postnatal days 0, 5, and 10.

Runx2 expression was up-regulated by miR-exon4 mimic in LS8 cells

We transfected the miR-exon4 mimic into the LS8 ameloblast-like cells to see the change in expression of genes related to ameloblast differentiation. We chose genes that are known to be upregulated from pre-secretory to secretory ameloblasts, including *Runx2* (Bronckers et al., 2001), *Satb1* (Zhang et al., 2014), *Tgfbr2 and Wnt10b* (identified in our preliminary qPCR and immunohistochemical screening). Transfection of the mature miR-exon4 mimic significantly induced expression of *Runx2*, but not *Wnt10b, Tgfbr2 and Satb1* (Fig 6).

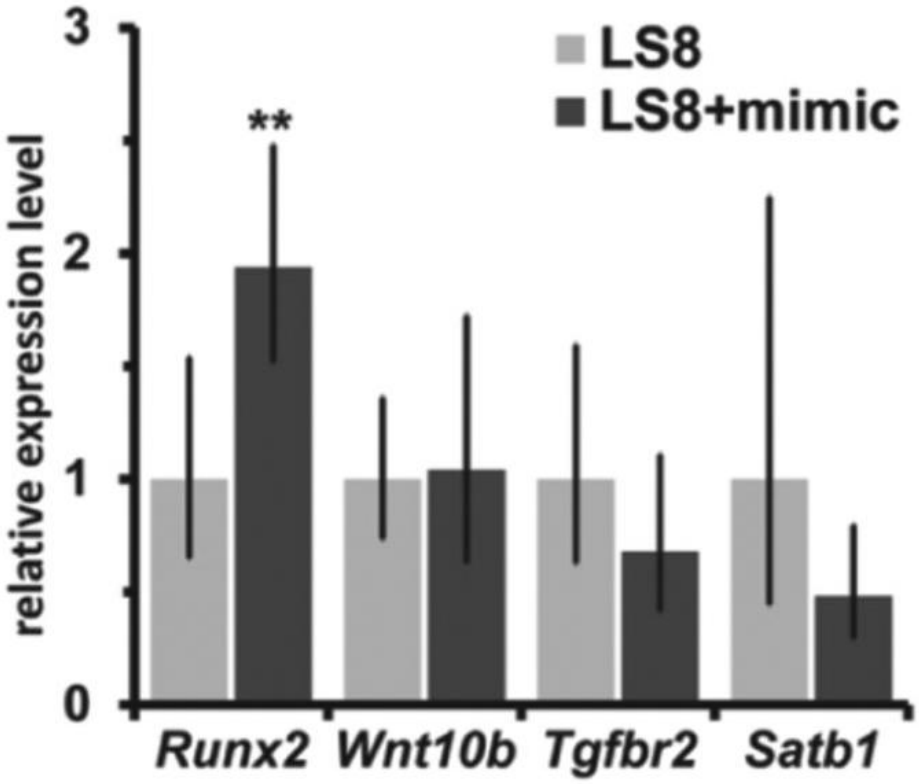

Figure 6 *Runx2 expression was up-regulated by miR-exon4 mimic in LS8 cells*
Change in expression of genes that may regulate ameloblast differentiation, after transfection of mature miR-exon4 mimic in LS8 cells. Transfection of miRNA mimic in LS8 cells significantly ($P < 0.01$) upregulates *Runx2* expression but not *Wnt10b*, *Tgfbr2*, and *Satb1* expression. Expression of mRNAs is demonstrated as the relative expression (fold change) level compared with untransfected control. Each bar represents a 95% confidence interval. **$P < 0.01$, $n = 9$ in each group.

miR-exon4 was expressed but significantly downregulated in Amel KO mice

Amel KO mice are known to show severe inhibition in enamel matrix formation due to lack of amelogenin protein synthesis attributed to an disruption on amelogenin gene at the border of exon2 and intron2 including signal peptide coding region of *Amel* (Gibson et al., 2001a). As Gibson's group reported, the *Amel* KO mice still produce some amelogenin mRNA variants skipping exon2 (Gibson et al., 2001a). Therefore, we determined whether miR-exon4 was produced in *Amel* KO mice, and found that indeed, the mature miR-exon4 was expressed in P0/pre-secretory and P5/secretory enamel organs of KO mice (Fig 7A). At P0, miR-exon4 expression was significantly increased in KO mice as compared to WT mice. However at P5, the expression level was significantly reduced, approximately 7.9% of WT. Despite the great reduction in expression, amelogenin mRNAs (containing exon6b-d, and exon4-6d) were still produced in *Amel* KO mice at a level of 1.10-3.14% of WT (Fig 7B-C).

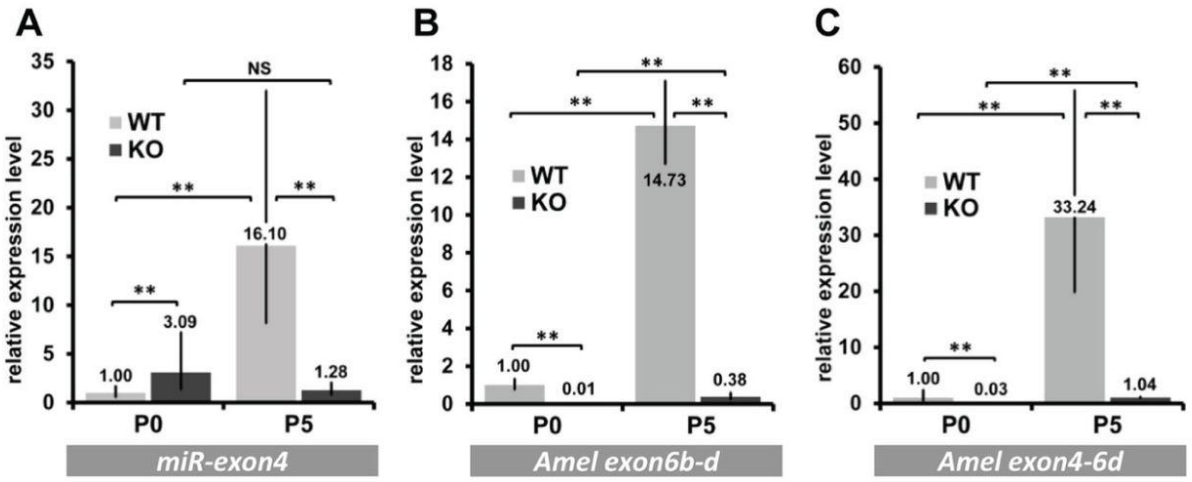

Figure 7 *miRNA derived from exon4 (miR-exon4) is expressed in Amel knockout (KO) enamel organ*
(**A**) miR-exon4 is expressed in both presecretory (P0) and secretory (P5) enamel organs of *Amel* KO mice. However, the expression level is greatly reduced at P5. Amelogenin mRNAs (containing exon6b-6d [**B**] and exon4-6d [**C**]) are also expressed in *Amel* KO mice, but its expression level is repressed at an even lower level compared with miR-exon4. Expression of miRNA or mRNAs is demonstrated as the relative expression (fold change) level compared with P0 wild type (WT). Each bar represents a 95% confidence interval. The significance of differences was determined by the 2-tailed multiple *t* test with Bonferroni correction following 2-way analysis of variance (4 comparisons in 4 groups).
**P* < 0.05, ***P* < 0.01, *n* = 4 in each group. *Abbreviations: P0, P5: postnatal days 0, 5.*

Ameloblasts in the Amel KO mice were morphologically similar to WT ameloblasts, with the exception of poorly formed Tomes' process (Fig 8B). Though the lack of secreted amelogenin protein resulted in thin enamel matrix (Fig 8B), transcriptions of mRNA for secretory enamel matrix proteins (*Ambn* and *Enam*) and proteinase (Mmp20) were similar to those of WT mouse ameloblasts (Fig. 8A).

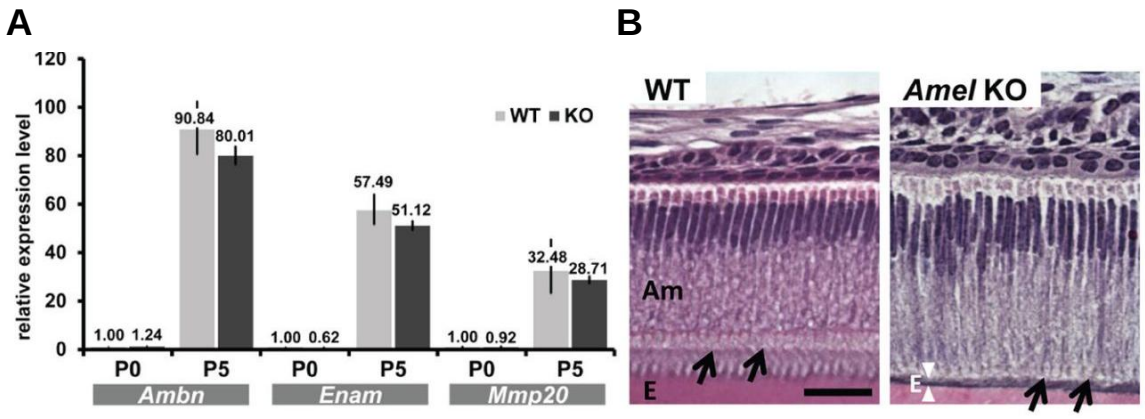

Figure 8 *Ameloblasts from amel knockout (KO) mice are similar to WT mice*
(**A**) mRNA expression of the major enamel matrix proteins in enamel organs (*Ambn, Enam,* and *Mmp20*) is not significantly changed in *Amel* KO at any stage. Expression of miRNA or mRNAs is demonstrated as the relative expression (fold change) level compared with P0 WT. Each bar represents a 95% confidence interval. The significance of differences was determined by the 2-tailed multiple *t* test with Bonferroni correction following 2-way analysis of variance (4 comparisons in 4 groups). *n* = 4 in each group.

(**B**) In *Amel* KO mice, enamel matrix formation is highly reduced (arrowheads). Except the disruption in Tomes' process formation (arrows), alteration in ameloblast morphology is not evident at the secretory stage.
Abbreviations: Am, ameloblast; E, enamel matrix. Bar: 25 μm.

Reduction of miR-exon4 resulted in downregulation of Runx2 in Amel KO mice

To determine the biological significance of miR-exon4 in amelogenesis, we further analyzed the expression of differentiation associated genes (*Runx2, Wnt10b, Tgfbr2* and *Satb1*) in the enamel organ of *Amel* KO mice where miR-exon4 expression was downregulated (Fig 7A). As *in vitro* transfection of miR-exon4 mimic indicated the potential relation between *Runx2* and miR-exon4, we found that *Runx2* expression was significantly reduced in P5 *Amel* KO secretory enamel organ as compared to WT mice (Fig 9). Unlike in LS8 cell, expression of *Wnt10b* and *Satb1* were also downregulated in *Amel* KO enamel organ compared to WT mice (Fig 9).

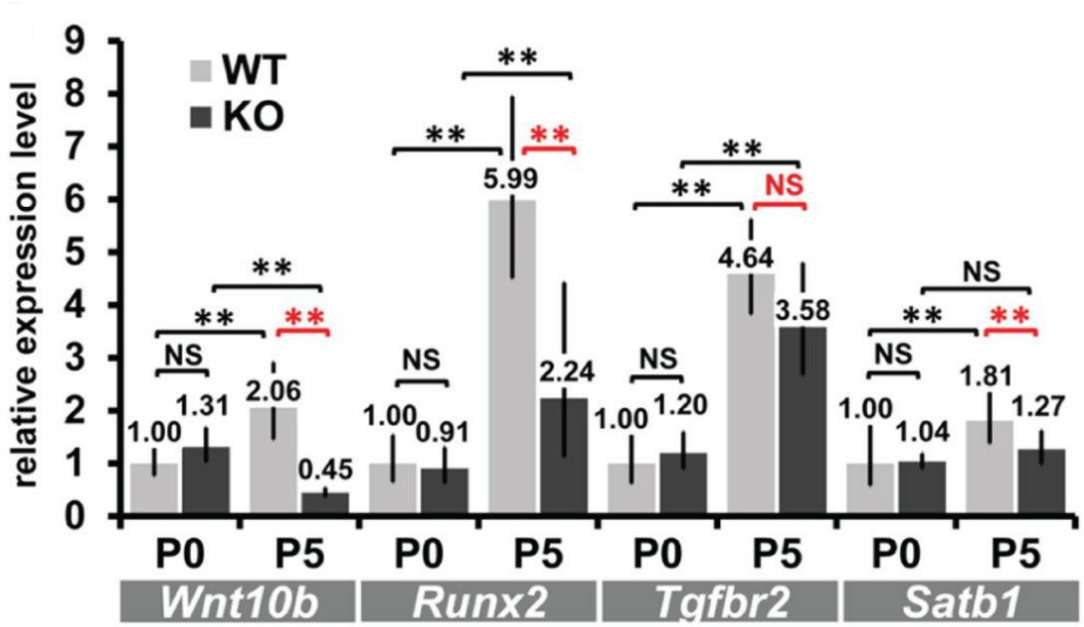

Figure 9 *Expression of Runx2 is downregulated in Amel knockout (KO) enamel organ at the secretory stage (P5)*
In wild-type (WT) enamel organ, expression of the signal regulative genes (*Wnt10b, Runx2, Tgfbr2*, and *Satb1*) increases toward the secretory stage (P5). At P0, none of the genes change in their expression level, while at P5, expression of *Runx2, Wnt10b*, and *Satb1* is significantly reduced in *Amel* KO mice. Expression of miRNA or mRNAs is demonstrated as the relative expression (fold change) level compared with P0 WT. Each bar represents a 95% confidence interval. The significance of differences was determined by the 2-tailed multiple *t* test with Bonferroni correction following analysis of variance (4 comparisons in 4 groups). **P* < 0.05, ***P* < 0.01, *n* = 4 in each group. P0, P5: postnatal days 0, 5. NS, not significant.

Downstream targets of Runx2 were downregulated in Amel KO enamel organ

To further confirm the significance in reduction of *Runx2* in *Amel* KO mice, we examined the expression of genes downstream of Runx2; *Odam* and *Amtn* (Lee et al. 2010, Xiaoying and Yuguang 2013). Expression of these genes was significantly downregulated at P5 in *Amel* KO as compared to WT (Fig 10A). Interestingly, the morphology of ameloblasts in maturation stage, where generally amelotin protein was observed on the basal lamina (Somogyi-Ganss et al., 2012), was also notably disorganized in the KO mice (Fig 10B).

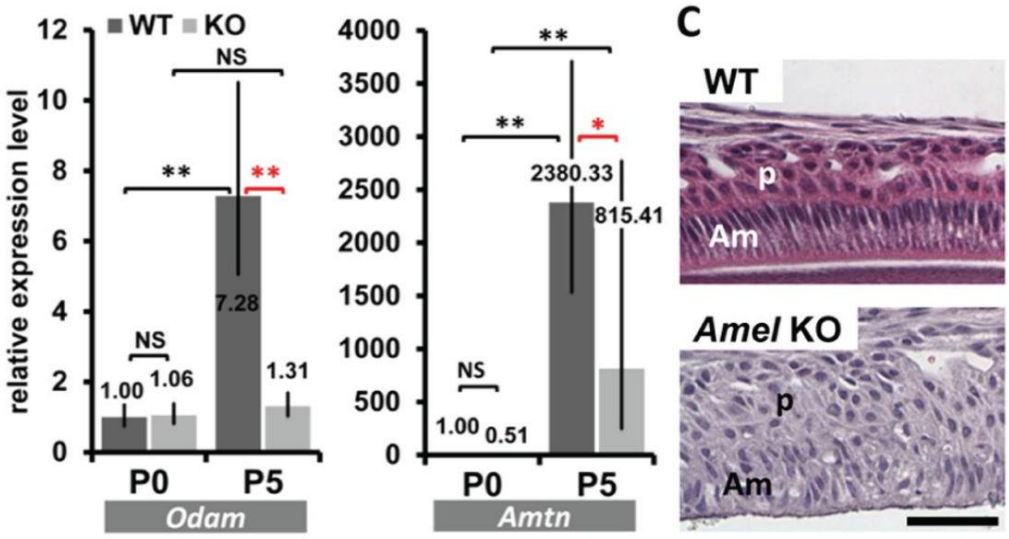

Figure 10 *Expression of Runx2 is downregulated in Amel knockout (KO) enamel organ at the secretory stage (P5)*
(A) In WT enamel organ, expression of the known RUNX2 downstream targets (*Odam* and *Amtn*) increases from presecretory (P0) to secretory (P5) stages similar to *Runx2*. The expression was significantly downregulated in *Amel* KO mice at the secretory stage (P5). Expression of miRNA or mRNAs is demonstrated as the relative expression (fold change) level compared with P0 WT. Each bar represents a 95% confidence interval. The significance of differences between P0 WT and other values was determined by the 2-tailed multiple *t* test with Bonferroni correction following analysis of variance (4 comparisons in 4 groups). $^{**}P < 0.01$, $n = 4$ in each group.

(B) Hematoxylin and eosin staining of early maturation ameloblasts shows disorganized ameloblasts and papillary layer in *Amel* KO mice.
Abbreviations: Am, ameloblast; P, papillary layer. Bar: 25 μm.

2.4 Discussion

In this study, we determined that a novel miRNA (miR-exon4) was produced from amelogenin exon4. We found that amelogenin transcripts that included exon4 comprised approximately 20% of amelogenin splice variants at all stages of enamel formation, indicating that exon4 was mostly spliced out and available for miRNA processing. In the *Amel* KO mice, where the total amelogenin mRNA expression was reduced, miR-exon4 expression was also reduced. *In vitro,* when LS8 cells were transfected with an amelogenin minigene, miR-exon4 was increased. These results indicate that in the enamel organ, miR-exon4 is produced along with amelogenin mRNAs through transcription and alternative splicing.

Amelogenin exon4 is a unique exon compared to other exons, as it appeared and became functional later in placental evolution. Its sequence is highly conserved in all primates and rodents. In mice, an identical exon of exon4 is present in intron7 as exon4b (Sire et al., 2012). The sequence of intron4 includes a conserved CNNC motif in the intron7 downstream the exon4b (Figure 11). Therefore, in mice, this exon4b could be an additional source of miR-exon4.

Since expression of miR-exon4 level was the highest at the secretory stage, we investigated correlation of miR-exon4 and ameloblast differentiation into the secretory stage by examining the expression of several genes known to be associated with differentiation of secretory stage ameloblasts. *In vitro,* after transfection of an amelogenin minigene, we found that *Runx2* expression, but not *Satb1, Wnt10b or Tgfbr2,* was altered in association with miR-exon4. *In vivo,* we also found that in the *Amel* KO mouse model, where miR-exon4 was reduced, *Runx2* expression was also significantly reduced.

An increase in the level of *Runx2* expression level with ameloblast maturation suggests a specific role of RUNX2 in ameloblast differentiation (Bronckers et al., 2001). RUNX2 has been shown to regulate both ODAM expression and *Amtn* promoter activity (Lee et al., 2010; Xiaoying and Yuguang, 2013), both of which are upregulated during ameloblast differentiation, with maximum expression at the maturation stage (Fukumoto et al., 2014). Interestingly, we found that *Odam and Amtn* were also reduced in *Amel* KO mice at the secretory stage, while other matrix proteins and proteinases including *Ambn, Enam,* and

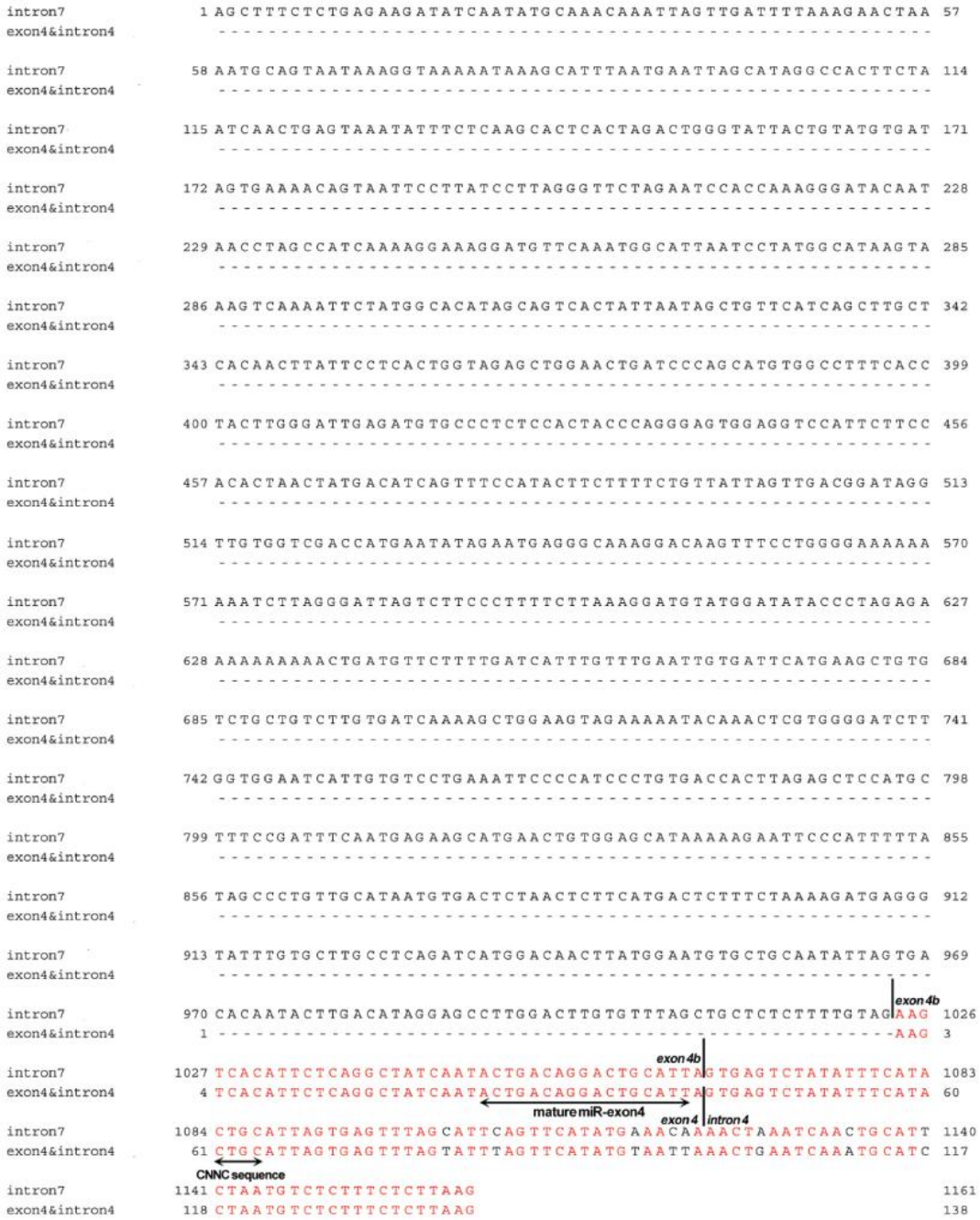

Figure 11 *Alignment of intron7 vs. exon4 and intron4 in mouse amelogenin gene (gene ID 11704)*

Mmp20 were not altered. It may be that beginning in the secretory stage, an increase in miR-exon4 results in an upregulation of *Odam* and *Amtn* expression, which then continues into maturation. Indeed the altered ameloblast morphology in the maturation stage of *Amel* KO mice, which have reduced miR-exon4 and *Runx2* expression supports this possibility.

Though *Amel* KO ameloblasts do differentiate, we did some significant morphological differences, including lack of Tomes' processes in the secretory stage, possibly related to the lack of secreted amelogenins and reduced expression of miR-exon4. Unlike our *in vitro* results, we found that *in vivo*, expression of *Wnt10b* and *Satb1* was also reduced in *Amel* KO mice as compared to the WT. In the bone marrow stromal cell line, *Wnt10b* expression has been shown to be regulated by the alternatively spliced amelogenin M59 amelogenin, known as LRAP (Wen et al., 2011), suggesting that the downregulation in *Wnt10b* in the *Amel* KO enamel organ is due to reduced LRAP and/or other amelogenin proteins, rather than an effect on miR-exon4.

All these data suggest that miR-exon4 functions as a regulator of *Runx2* during ameloblast and osteoblast differentiation. However, miRNAs function through inhibiting translation or inducing degradation of target mRNAs, and therefore the expression profile of miRNAs and their direct targets are expected to be opposite. In this study, expression of *Runx2* was directly related to miR-exon4, as in the *Amel* KO enamel organ where miR-exon4 was expression of was reduced, *Runx2* was also significantly downregulated, and when miR-exon4 was increased *Runx2* was also increased. Therefore, it appears that miR-exon4 indirectly regulates *Runx2* by inhibiting expression of a yet unknown gene by miR-exon4. In fact, an Ingenuity Pathway Analysis (Qiagen) correlated *Runx2* and multiple genes predicted as the potential direct targets of miR-exon4 by DIANA microT 3.0 (Selbach et al., 2008) (data not shown). Further investigations of these genes as a possible direct target of miR-exon4 are underway, and will add to our understanding of amelogenin transcription, including the formation of miR-exon4 and amelogenesis.

Chapter 3
Fluoride Downregulates Klk4 Expression Through Inhibition of Androgen Receptor Activation

3.1 Introduction

Dental enamel is the highly mineralized protective outer covering of teeth, conferring strength, abrasion resistance, and protection of the teeth in the oral cavity (Shimizu and Macho, 2008). Its formation, called amelogenesis, occurs in two major stages: secretory and maturation. In the secretory stage, an enamel protein matrix is synthesized to support elongating enamel crystals that thicken in maturation stage. Crystal thickening in maturation stage begins after the enamel matrix reaches its final thickness, and occurs as matrix proteins are hydrolyzed and removed to create space for the growing crystals. If this hydrolysis is inhibited, the mineralized enamel has increased protein content, resulting in hypomineralized or hypomature enamel with discoloration and/or flaking (Den Besten, 1986; Simmer et al., 2009). This outcome affects the psychosocial development of children at a crucial age of their development (Coffield et al., 2005; Welbury and Shaw, 1990).

Kallikrein-related peptidase 4 (KLK4) is the primary protease of maturation-stage amelogenesis and responsible for final hydrolysis of the enamel matrix (Lu et al., 2008). KLK4 is secreted by ameloblasts, and the highest levels of *Klk4* expression occurs during the maturation stage (Hu et al., 2002; Simmer et al., 2009). *In vivo*, maturation-stage ameloblasts (MAB) with inactivated transforming growth factor-beta receptor 2 (TGFBR2) or exposed to excess levels of fluoride have decreased *Klk4* expression (Cho et al., 2013; Suzuki et al., 2014). Fluoride enhances mineral formation, and it is possible that the effects of fluoride on *Klk4* expression by ameloblasts are in response to fluoride-related extracellular changes in the enamel matrix. Despite the importance of KLK4 in final enamel mineralization, the mechanisms by which ameloblasts regulate Klk4 expression in ameloblasts are not known, and the decrease in KLK4 expression in the presence of fluoride offers the possibility of further understanding how KLK4 is regulated during enamel formation.

In other cells and tissues, *Klk4* expression is known to be upregualted in response to activation of androgen receptor (AR). In prostate cancer cells, AR is an intracellular receptor that becomes a nuclear-translocating transcription factor upon binding to androgen hormones, leading to an upregulation of *Klk4* expression (Lai et al., 2009). In MAB, *Klk4* transcription has been shown to be upregulated by exogenous TGF-β_1 (Suzuki et al., 2014), which activates AR in prostate cancer cells (Yang et al., 2014). The link between AR and TGF-β signaling in MAB is further demonstrated that the exposure of rats to the same levels of fluoride that suppresses TGF-β signaling in MAB leads to serum androgen hormone levels being significantly reduced (Zhou et al., 2013). These data imply AR signaling is an intracellular mediator for *Klk4* transcription in MAB. To explore this possibility, we used both *in vivo* and *in vitro* studies to determine whether AR signaling regulates *Klk4* expression in ameloblasts and if this signaling can be extracellularly modulated in ameloblasts, by fluoride-related changes in the extracellular matrix.

3.2 Materials and Methods

Animals

All animal procedures were carried out with approval by the University of California-San Francisco Institutional Animal Care and Use Committees. The experiments reported herein were conducted in compliance with the Animal Welfare Act and in accordance with the principles set forth in the National Research Council's *Guide for the Care and Use of Laboratory Animals*.

Three-week-old female Wistar rats (Jackson Laboratory, Sacramento, CA) were divided into two groups, with the groups given either deionized drinking water or deionized drinking water supplemented with 100 ppm fluoride as sodium fluoride (Sigma-Aldrich, St. Louis, MO) *ad libitium* for four weeks. After six weeks, the rats were euthanized, the mandibles dissected and alveolar bone removed to allow access to separately dissected the enamel matrix and enamel organ for KLK4 activity assays, and quantitative real-time polymerase chain reaction (qPCR) of the relative expression of *Klk4* mRNA.

Three-week-old C57BL/6J mice (Jackson) were divided into two groups, with the groups given either deionized drinking water or deionized drinking water supplemented with 50 ppm fluoride as sodium fluoride (Sigma-Aldrich) *ad libitium* for four weeks. After four weeks, they were euthanized, and mandibles were obtained for morphology, immunohistochemical analyses, and qPCR of incisors. We used 50 ppm fluoride levels for mice to generate serum fluoride levels that would be similar to levels seen in humans exposed to 5 ppm fluoride (Guy W et al., 1976).

Seven-week mice with impaired AR function due to lack of steroid and DNA binding domains caused by frameshift mutation (Ar^{Tfm}) (He et al., 1991) were purchased (Jackson), euthanized, and the mandibles obtained for morphology.

KLK4 activity assay

Rat mandibular incisors were removed from the alveolar bone and enamel matrix was dissected from the underlying dentin surface at the early-maturation stage. This includes enamel matrix underlying the distal

root of the first molar and continuing until the enamel was too hard to dissect (Stahl et al., 2015). Extracts were homogenized in 100ul of 5% TCA, and incubated at room temperature for 30 min. After centrifugation at 10,000 G for 10 minutes, the supernatants were removed and pellets were resuspended in 200uL of ammonium bicarbonate. The total protein concentration of each sample was measured by Braford assay. KLK4 activity was analyzed by using Boc-Val-Pro-Arg-AMC fluorogenic peptide substrate (R&D Systems Inc., Minneapolis, MN). Each reaction in 96-well black plates contained 150 µL of protein extracts, 5 µL of peptide and 40 µL of 5x reaction buffer (250 mM Tris–HCl , 250 mM NaCl, 50 mM CaCl). The fluorescence signal was detected using a spectrometer at 37°C (excitation at 380 nm and emission at 460 nm), and measured every 20 min for 180 min. For each sample, the fluorescence data was normalized to the protein concentration for a given sample. For each sample, we used R software environment with *drc* package (Ritz and Streibig, 2005; Team, 2014) to generate an averaged 4-parametric regression curve of the treatment groups. Significance of differences at 60, 120, and 180 min were determined by independent Student's t-test.

qPCR analysis

Total RNA was isolated from (rat and mouse) mandibular maturation-stage incisor enamel organs that were dissected according to landmarks described previously (Stahl et al., 2015), and also from ALCs (See below) using RNeasy Mini kit (Qiagen, Germantown, MD). Conversion of mRNA to cDNA was obtained by reverse transcription of the mRNA using Superscript III First-Strand Synthesis Supermix for qRT-PCR (Life Technologies, Carlsbad, CA).

Expression of mRNAs was examined by qPCR with FastStart Universal SYBR Green Master Kit (Roche Diagnostics, Indianapolis, IN) using primer sets for *Klk4, Ccnd1, Ar, Tgfbr2, and Tgfb1* (Elim Biopharmaceuticals, Hayward, CA). *Mrpl19* was used as a reference gene for enamel organ samples and *Eef1a1* for ALCs. Primer sequences are listed in Appendix 3. The relative expression level of target genes was analyzed by the ΔΔCt method (Livak and Schmittgen, 2001). Expression of each gene was calculated as a relative expression level (fold change) compared with WT (mice samples) or untreated controls (cell

culture). Significance of differences was determined using ΔCt values by the two-tailed multiple t-test with Benjamini & Hochberg correction following ANOVA (Benjamini and Hochberg, 1995).

Immunohistochemistry

Mouse mandibles were dissected from other samples, and fixed in 4% paraformaldehyde in 0.06M sodium cacodylate buffer (pH 7.3) at 4°C for 24 hours. After decalcification in 8% EDTA (pH 7.3), samples were processed for routine paraffin embedding and sagittally sectioned. The sections were incubated with 10% swine and 5% goat sera followed by incubation with rabbit anti-human AR (1:75; Novus Biologicals, Littleton, CO, NB100-91658), rabbit anti-mouse TGFBR2 (1:100; Santa Cruz Biotech, Santa Cruz, CA), rabbit anti-human TGFB1 (1:50; Abcam PLC, Cambridge, MA, ab92486) antibody overnight at room temperature. A biotinylated swine anti-rabbit IgG F(ab′)2 fraction (Dako, Carpinteria, CA) was used as the secondary antibody for 1 hour at room temperature incubation. Following incubation with alkaline phosphatase conjugated streptavidin (Vector Laboratories Inc., Burlingame, CA) for 30 min, immunoreactivity was visualized using a Vector® Red kit (Vector) resulting in pink/red color for positive staining. Counter-staining was performed with methyl green (Dako). Negative control was done with normal rabbit sera.

Cell culture

Mouse ameloblast-lineage cells (ALCs, a kind gift from Dr. Toshihiro Sugiyama, Akita University, Japan and Dr. John Bartlett, Forsyth Institute, Boston, Massachusetts) (Nakata et al., 2003) were cultured in DMEM (UCSF Cell Culture Facility, San Francisco, CA) supplemented with 10% Fetal Bovine Serum (FBS) (Gemini Bio-Products, West Sacramento, CA) and 1% penicillin-streptomycin. ALCs (2.0×10^5) were seeded into 6-well plates. After 24 hours, the cells were treated with fluoride (0, 10, 100, 1000 μM) as sodium fluoride (Sigma-Aldrich), and followed by total RNA extraction. The extracts were analyzed for *Klk4*, *Ar*, *Tgfb1*, *Tgfbr2*, and *Ccnd1* expression.

3.3 Results

Rats given 100 ppm F in drinking water had reduced matrix KLK4 proteolytic activity and reduced Klk4 expression by maturation stage ameloblasts

Fluorosed enamel matrix protein extracts had lower overall KLK4 activity profile, and at 60, 120, and 180 minutes of incubation, the activity was significantly lower compared to controls (Fig 12A). Consistent with the reduced proteolytic activity in the enamel matrix, Klk4 mRNA expression was also significantly reduced (Fig 12B).

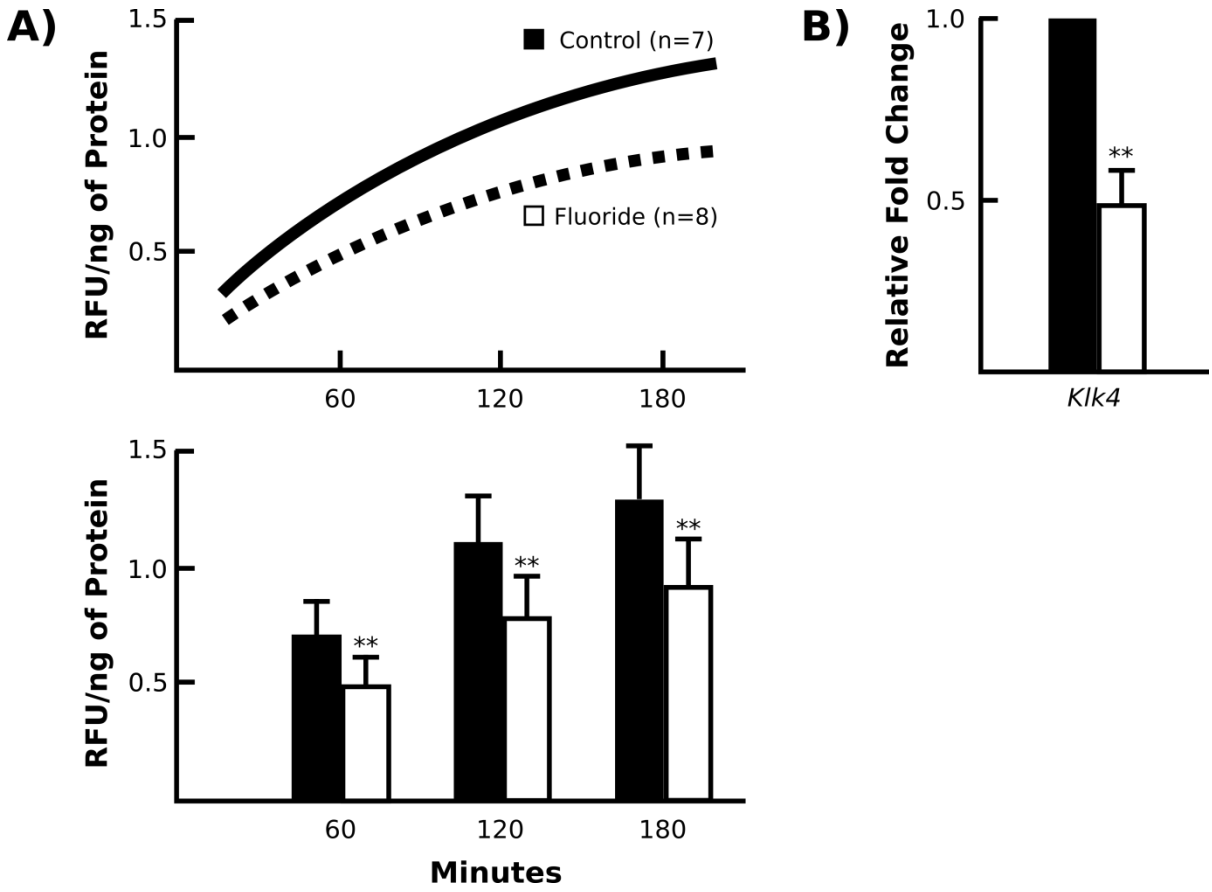

Figure 12 *Fluoride decreased in vivo KLK4 activity and Klk4 expression.*
(A) Averaged profile model of KLK4 activity in early maturation enamel matrix protein extracts (line graph). At three time points of measurement (60, 120, and 180 minutes after start of incubation), fluorosed enamel showed significantly lower KLK4 activity (bar graph). ** $p < 0.01$ (B) Relative fold change of Klk4 expression from maturation-stage enamel organs harvested from control and fluorosed rats. Fold change was calculated relative to the baseline expression of the gene in control mice. Genes were normalized to the expression of Mrpl19 (mouse ribosomal protein L19). ** $p < 0.01$

The maturation stage enamel matrix was retained in both fluoride treated and Ar^{Tfm} mice as compared to wildtype

As previously reported (Everett et al., 2009), mice given high levels of fluoride in drinking water, had retained enamel matrix (Fig 13A-B). qPCR analysis confirmed that similar to rats, mice had reduced *Klk4* expression (data not shown). Since AR has not been previously found in the ameloblasts, I immuno-localized AR in ameloblasts and found AR localized in the nucleus of mice (Fig 2C). I found reduced AR translocation to the nucleus in the fluoride treated mice (Fig 2E). When I examined incisors Ar^{Tfm} of mice, I found that enamel matrix was also retained, similar to what I found in fluoride treated mice (Fig 13C).

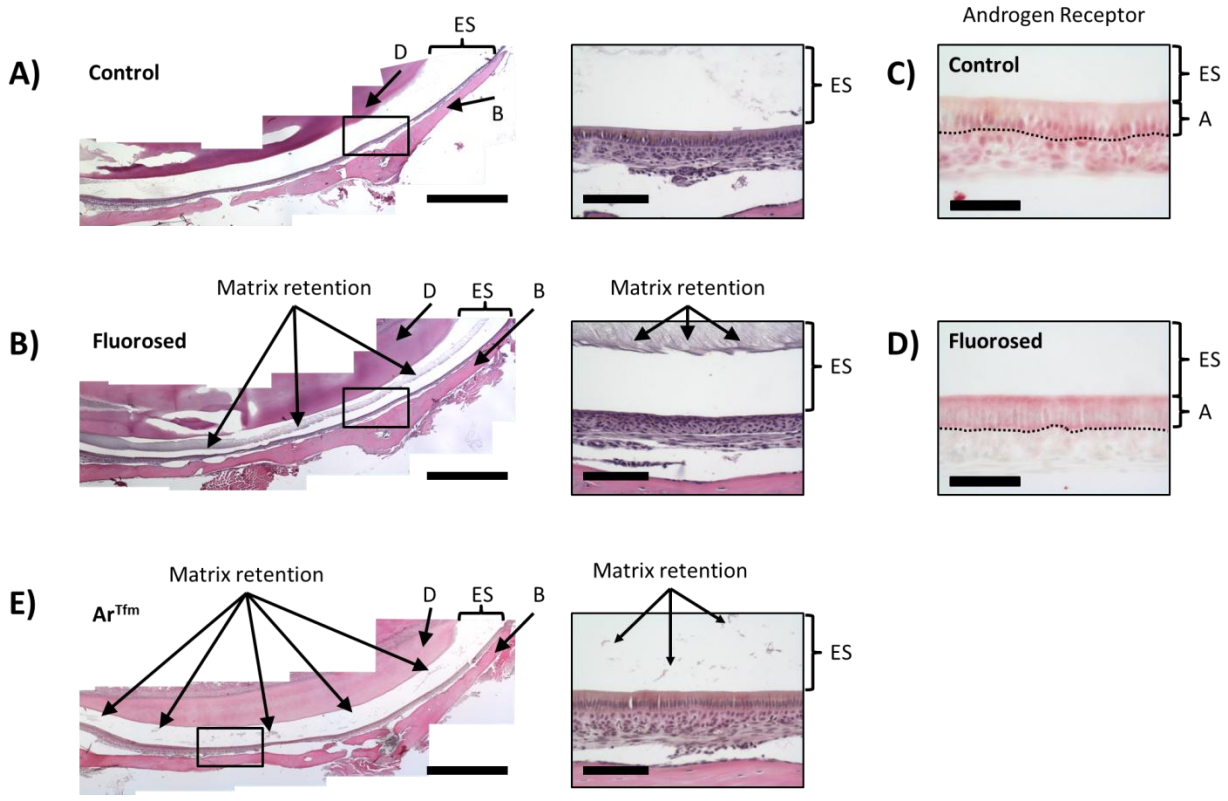

Figure 13 *Ar^{Tfm} mice exhibit enamel matrix protein retention similar to fluoride exposed mice*
(A-B,E) Composite images of hematoxylin and eosin-stained mandibular incisors from control, fluorosed, and Ar^{Tfm} mice. Retained enamel matrix protein is seen in the enamel space of fluorosed and Ar^{Tfm} unlike control mice. Denoted black boxes in the composite image are magnified. Composite scale bar 1 mm. Magification scale bar 100 um
(C-D) Images of maturation-stage ameloblasts stained with anti-AR red immunostaining and counter-stained with methyl green from control (C) and fluorosed (50 ppm F) (D) mice. While control mice have positive immunostaining in the nucleus, it is noticeably less intense in fluoride-exposed maturation-stage ameloblasts. Scale bar 50 um
Abbreviations: ES – enamel space, A – maturation ameloblast, P – papillary layer, B – bone

Decreased AR activation in ameloblasts was related to increased expression of Cyclin D1

We used our fluorosis model to further explore the regulation of *Klk4* expression through the AR in ameloblasts by analyzing both cyclin D1 (*Ccnd1*) and *Tgfbr2* expression in maturation stage ameloblasts. Expression of Ccnd1 was significantly upregulated, and *Tgfbr2* was significantly downregulated in fluoride-exposed MAB compared with the controls (Figure 14A). Immunostaining for TGFBR2 and TGFB1 were both reduced in fluoride-exposed maturation ameloblasts (Figure 14B).

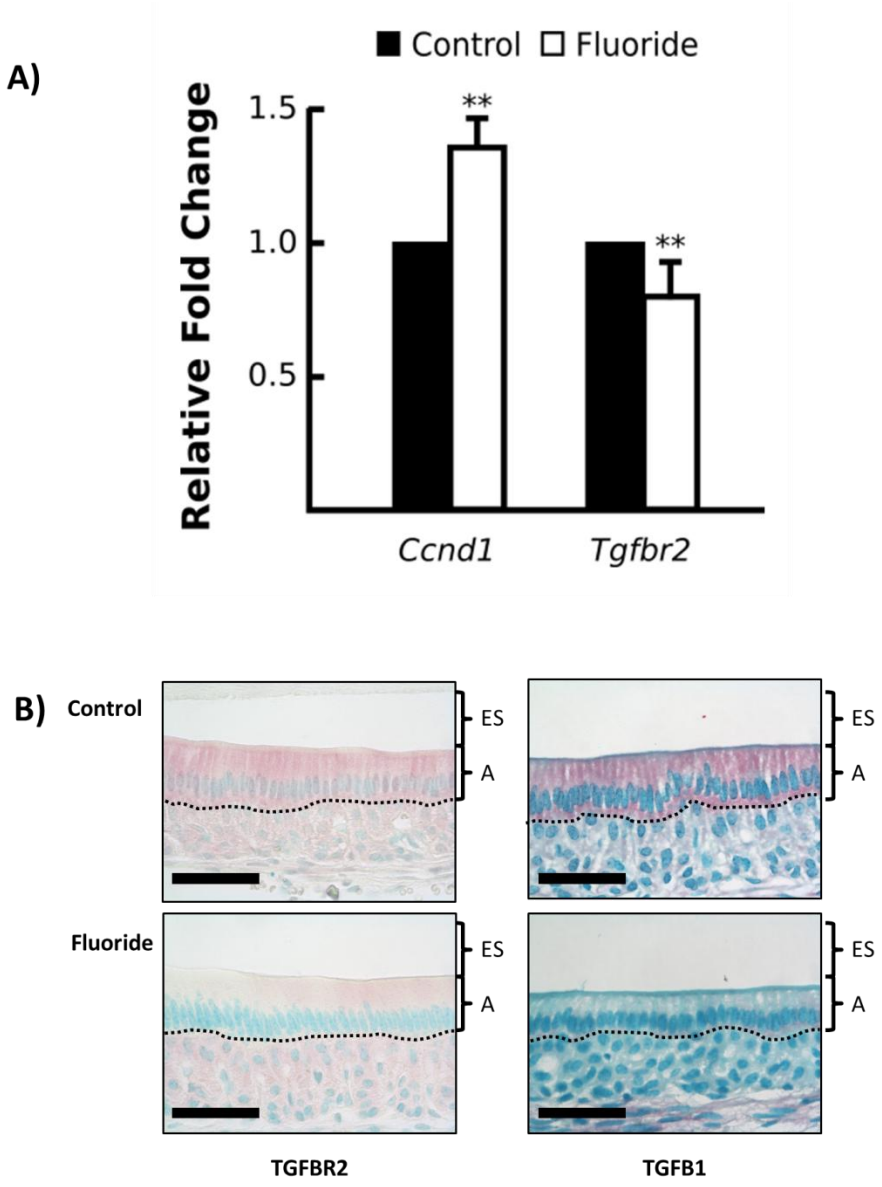

Figure 14 *Fluoride altered expression CCND1 and TGFBR2, regulators of androgen receptor activation*
(A) Relative fold change of CCND1 and TGFBR2 expression from maturation-stage ameloblasts harvested from control and fluorosed mice. Fold change was calculated relative to the baseline expression of the gene in control mice. Genes were normalized to the expression of Mrpl19 (mouse ribosomal protein L19). ** $p < 0.01$
(B) Images of red TGFBR2 and TGFB1 immuno-histochemical staining show fluoride-exposed MAB have decreased amounts of TGFBR2 and TGFB1 protein compared to controls. Scale bar 50 um
Abbreviations:
ES – enamel space,
A – maturation ameloblast

Fluoride did not alter Klk4 or Ar expression in vitro at near physiologic serum fluoride levels

Klk4 expression in ALC exposed to fluoride was significantly reduced at 100 and 1000 µM, but not at a high, but still physiologic serum fluoride level (10uM) (Fig 15). Fluoride did not significantly change *Ar* expression at 10, 100, and 1000 µM.

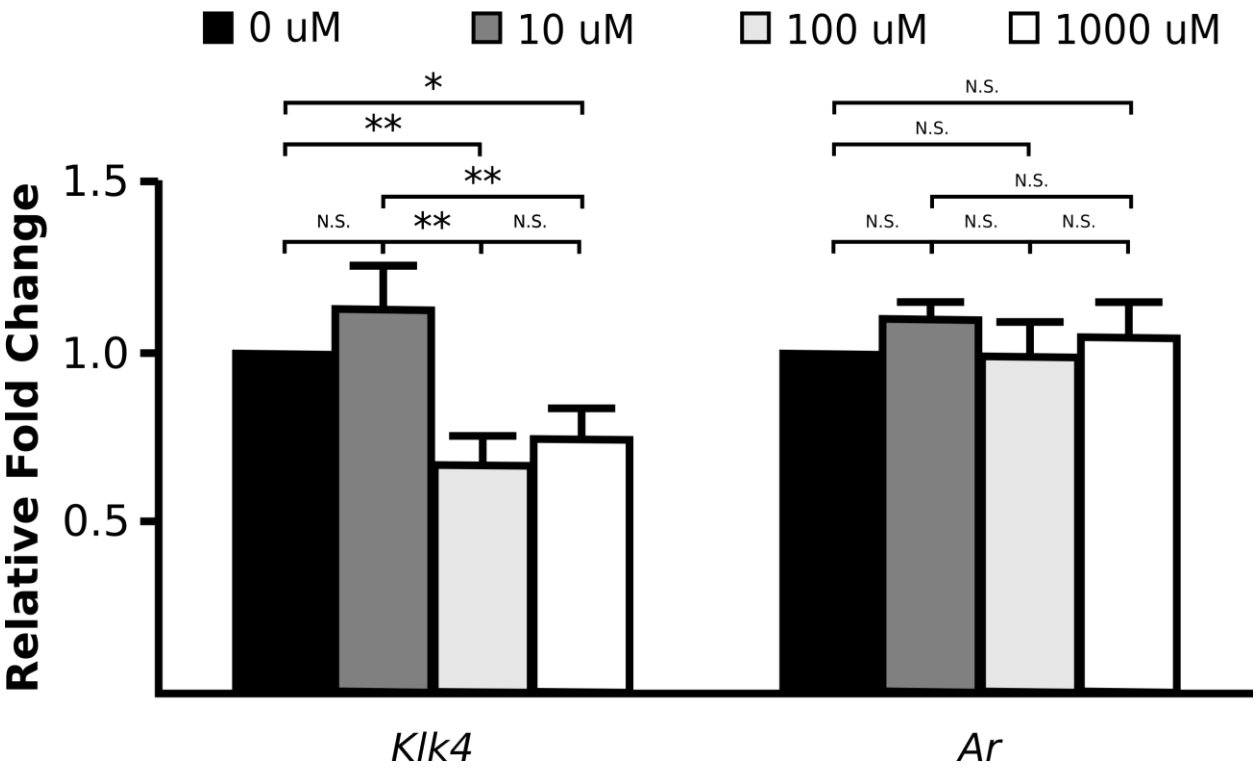

Figure 15 *Fluoride does not alter Klk4 or Ar expression at near physiologic serum fluoride levels.*
Relative fold change of *Klk4* and *Ar* from ameloblast-lineage cells (ALC) exposed to 0 (Control), 10, 100, or 1000 µM fluoride. Fold change was calculated relative to the baseline expression of the gene in control mice. Genes were normalized to the expression of L19 (mouse ribosomal protein L19). * $p < 0.05$, ** $p < 0.01$

3.4 Discussion

KLK4 is known to be the major matrix proteinase produced by maturation ameloblasts, and is thought to be primarily responsible for the final degradation of enamel matrix proteins in maturation-stage enamel. The hypomineralized phenotype of severely fluorosed enamel is thought to be in part due to a prolonged retention of enamel matrix proteins (Den Besten, 1986; Wright et al., 1996), likely related to the reduced proteinase activity in fluorosed maturation stage enamel (DenBesten et al., 2002). Free fluoride in the enamel matrix is at micromolar levels (Aoba, 1997), which does not significantly alter matrix proteinase activity (Tye et al., 2011). However, Suzuki et al. reported the reduced *Klk4* transcripts in the enamel organ of rats exposed to 50-100 ppm fluoride in the drinking water (Suzuki et al., 2014), suggesting that reduced proteinase activity may be due to a specific effect on KLK4 synthesis. In this study, we confirmed that fluoride not only reduced KLK4 activity in maturation enamel matrix *in vivo*, but also a down regulated *Klk4* expression in maturation enamel organ. Furthermore, the data suggests that fluorosis is a useful model to study *Klk4* regulation in ameloblasts. We confirmed that the 50 ppm F fluorosed mouse model exhibited retained enamel matrix through histomorphology analysis. In addition, we found the mouse maturation enamel organ from mice exposed to 50 ppm F expressed reduced *Klk4* transcripts similarly to rat maturation enamel organ exposed to 100 ppm F.

KLK4 is one of 15 human KLKs (Ramsay et al., 2008), and besides teeth, its mRNA is also detected in the normal prostate (Nelson et al., 1999; Simmer et al., 2011). KLK4 is also associated with androgen-induced prostate cancer progression (Klokk et al., 2007) , as androgen-driven androgen receptor (AR) signaling increases *Klk4* expression (Nelson et al., 1999). The mechanism(s) responsible for directly regulating *Klk4* expression in ameloblasts is not known, and therefore, we determined whether AR is present in ameloblasts and if it regulates KLK4. This is the first study to confirm that AR was expressed by ameloblasts and that fluoride can affect its translocation into the nucleus. Furthermore, mutating AR to be unable to bind to androgens (i.e. Ar^{Tfm} mice) resulted in increased enamel matrix retention. More of the matrix was retained in the fluorosed enamel matrix as compared to the Ar^{Tfm} maturation stage enamel

matrix, suggesting that the etiology of matrix retention in fluorosis results from additional mechanisms; likely also the effect of fluoride on pH modulation as the matrix mineralizes (Lyaruu et al., 2014).

Several reports have suggested the regulation of *Klk4* expression by AR signaling is an indirect process (Lai et al., 2009), including regulation by Cyclin D1 (CCND1). CCND1 is a protein commonly known for regulating cell cycle dynamics, and is a known negative regulator of AR, not only by directly binding to AR to inhibit activation of AR, but also by attenuating AR-induced upregulation of *Klk4* in prostate cancer (Comstock et al., 2011; Knudsen et al., 1999). Supporting this, our study also detected increased *Ccnd1* expression in fluorosed maturation ameloblasts, and therefore, suggests that AR signaling is an intracellular regulator for *Klk4* transcription in maturation ameloblasts.

Other studies reported an increase of *Klk4* expression in an androgen-dependent prostate cancer cell line (LNCaP) after exposure to TGF-β_1. In the maturation stage enamel organ, *Tgfb1* is decreased in fluorosed mice (Suzuki et al., 2014), and *Klk4* expression is decreased in ameloblasts of mice lacking *Tgfbr2* (Cho et al., 2013) suggesting a relationship between TGF-β signaling and *Klk4* expression in ameloblasts. TGF-β_1 is known to inhibit *Ccnd1* expression in intestinal epithelial cells (Ko et al., 1995), and hence, our finding of increased *Ccnd1* expression and decreased expression of both TGFBR2 and TGFB1 further support the possibility that fluoride related changes in *Klk4* expression is due to altered TGF-β signaling. *Tgfb1* expression is in part mediated by phosphorylation of c-Jun, as decreased c-Jun phosphorylation results in suppressed *Tgfb1* expression (Presser et al., 2013). We previously reported that physiologic fluoride levels reduce c-Jun phosphorylation *in vitro (*Zhang et al., 2007), so it may be possible that the effects of fluoride on TGFB1 and AR are related to the effect of phosphorylation of c-Jun.

To further determine whether fluoride could directly downregulate *Ar* expression, thereby downregulating *Klk4* expression, we added varying amounts of fluoride to ALC *in vitro*. Biologically relevant serum fluoride levels are in micromolar rather than millimolar concentrations, and humans drinking 3-5 ppm F (1 ppm F = 52.6 mM) fluoride supplemented water results in serum fluorosis with the serum fluoride

level around 3-5 µM (Guy W et al., 1976). In mouse, 50 ppm F in drinking water is known to result in approximately 5 µM serum fluoride (Zhang et al., 2014). However, many *in vitro* experiments employ millimolar levels of fluoride, which is 100 to 1000 times higher than that in serum of humans and rodents exposed to fluoride in drinking water. Such levels of fluoride are nephrotoxic and would not be encountered in daily life (Clark, 1977). In our *in vitro* studies, the amounts of fluoride added ranged from physiologic (10 µM) to above physiologic (100 and 1000µM), and although *Klk4* expression was decreased above physiologic levels, there was no effect at physiological fluoride levels.

Our cell culture model included the use of serum. In previous studies using serum-free medium, we found that fluoride could down regulate activate (phosphorylated) cJUN and c-JNK. However, some studies have shown that there are increased levels of c-Jun N terminal kinase (JNK) have been reported in serum (Mizukami et al., 2001). Therefore, it is possible that higher levels of fluoride are required to down regulate active c-JUN/JNK to effect a reduction in TGF-β expression, with a resultant increase of *Ccnd1* and reduced *Klk4* expression (Presser et al., 2013; Schwabe et al., 2003).

Another explanation for my finding that the androgen receptor is down regulated *in vivo*, in the presence of fluoride, is that fluoride downregulates androgens systemically. Zhou et al. have reported that female rats given 100-200 ppm F in drinking water resulted in a significant decrease in serum testosterone (Zhou et al., 2013). If fluoride does change the serum androgen level, activation of AR signaling would also be reduced, and as a result, less *Klk4* transcription is to be expected as well. However, further studies to determine whether lower levels of fluoride (i.e. resulting in serum levels of 5µM) can induce changes in androgen production, and the effects gender, genetic background and/or age are necessary.

While signaling effects of androgens are well understood in tissues related to male physiology and sexual development, its role in tooth development is still relatively unknown. Tooth formation predominantly occurs prior to the onset of sexual maturity (exception of secondary and tertiary permanent molars). However, there are reports of significant differences in tooth size between males and females, so it could

be possible that the presence of the AR receptor in tooth formation may be a factor in the significant increase in tooth size in males as compared to females (Adeyemi and Isiekwe, 2003; Lombardo et al., 2016).

Taken all together, my data supports the importance of both TGF-β signaling and AR in *Klk4* expression in ameloblasts. My *in vitro* data suggests that physiological levels fluoride may not have a direct effect on ameloblasts to downregulate AR activation. However, further studies on mice with different susceptibility to the effects of fluoride, are needed to determine whether these maturation stage related effects of fluoride are direct cellular effects or related to a more general effect of fluoride on ameloblast differentiation.

Chapter 4
Tracing Iron Transport Through Ameloblasts in Rodent Incisor Pigmentation

4.1 Introduction

Dental enamel from rodent incisors contains iron pigment (Halse, 1972b). This pigment appears on the enamel surface towards the end of amelogenesis, when the enamel has just about fully formed, and decreases the acid dissolution rate of the enamel (Halse and Selvig, 1974; Kato et al., 1988). Even though human teeth are not pigmented like rodents, this relationship between pigmentation and acid dissolution rate of enamel is of interest as several studies have been published to suggest an association between poor iron diets and increased incidence of severe early childhood caries (Bansal et al., 2016; Schroth et al., 2013; Tang et al., 2013).

Explorations into the mechanism behind rodent incisor pigmentation have focused on maturation ameloblasts, which appear to be the source of the pigment as these cells stain positive for iron during amelogenesis (Wen and Paine, 2013). Iron accumulation in maturation ameloblasts is prolonged or reduced in mice lacking genes that result in enamel hypomineralization (Muto et al., 2012; Yanagawa et al., 2004). However there are questions how is iron homeostasis regulated in maturation ameloblasts to deposit iron pigmentation on the enamel matrix.

Cells import iron through transferrin receptor (TFRC), store iron in ferritin (FT), and export out iron with ferroportin (FPN) (El Hage Chahine et al., 2011; Ward and Kaplan, 2012). Expression of these iron-related proteins is modulated by intracellular levels of iron that are unbound to protein, called labile iron pool (LIP) (Kakhlon and Cabantchik, 2002). The size of LIP is strictly regulated as a large LIP promotes the increased formation of reactive oxygen species (ROS) that produce oxidative damage biomolecules (Kruszewski, 2003). This happens because the iron found in LIP participates in redox reactions, alternating back and forth between its ferrous (Fe^{2+}) and ferric (Fe^{3+}) ionic forms and producing ROS in the process (McCord, 1998).

To understand the significance of iron homeostasis in maturation ameloblasts, I used mice exposed fluoride as an experimental model. Excessive *in vivo* exposure to fluoride results in reduced incisor pigmentation in mice strains susceptible to developing dental fluorosis. (Everett et al., 2002). Therefore, I used fluorosis models derived from fluoride-sensitive C57BL/6 to determine how iron travels through the ameloblast to be deposited on the enamel surface as an iron-base pigment on the enamel surface of rodent incisors. I hypothesized that in fluorosed maturation ameloblasts, intracellular iron levels are altered to promote iron retention, preventing iron release on to the enamel surface.

4.2 Materials and Methods

Section preparation

All animal procedures were carried out with approval by the University of California-San Francisco Institutional Animal Care and Use Committees. The experiments reported herein were conducted in compliance with the Animal Welfare Act and in accordance with the principles set forth in the National Research Council's *Guide for the Care and Use of Laboratory Animals*.

Three-week-old female C57BL/6J (C57) mice were divided into two groups, with the groups given either deionized drinking water or deionized drinking water supplemented with 50 ppm sodium fluoride (Sigma-Aldrich, St. Louis, MO) *ad libitium* for four weeks. After four weeks, the mice were euthanized and the mandibles dissected out and fixed in 4% paraformaldehyde in 0.06M sodium cacodylate buffer (pH 7.3) at 4°C for 24 hours. After decalcification in 8% EDTA (pH 7.3), samples were processed for routine paraffin embedding and sagittally sectioned.

Prussian blue staining for ferric (Fe^{3+}) iron

Potassium ferrocyanide, in the presence of hydrogen chloride, reacts with ferric (Fe^{3+}) iron forms an insoluble pigment known as Prussian blue (Wen and Paine, 2013). Paraffin sections were deparaffinized, rehydrated, and immersed in a freshly prepared solution made of equal parts of 10% potassium ferrocyanide and 20% hydrochloric acid for 5 minutes. Samples were then washed with distilled water, and counterstained with nuclear fast red, dehydrated, cleared with xylene and mounted with cover slips.

Immunohistochemistry

After deparaffinization and rehydration, longitudinal mandibular incisor sections from control (0 ppm F) or fluoride-exposed (50 ppm F) were incubated with 10% swine and 5% goat sera followed by incubation with rabbit anti-FTH1 (1:200; Santa Cruz Biotech, Santa Cruz, CA), anti-FTL (1:200; Abcam PLC, Cambridge, MA), anti-NFκB (p65) (1:500), anti-phosphorylated NFκB (p-p65) (1:200) anti-SOD1 (1:50), and anti-TFRC antibody overnight at room temperature. A biotinylated swine anti-rabbit IgG F(ab′)2

fraction (Dako, Carpinteria, CA) was used as the secondary antibody for 1 h at room temperature incubation. Following incubation with alkaline phosphatase conjugated streptavidin (Vector Laboratories Inc., Burlingame, CA) for 30 min, immunoreactivity was visualized using a Vector® Red kit (Vector) resulting in pink/red color for positive staining. Counter-staining was performed with methyl green (Dako). Negative control was done with normal rabbit sera.

Imaging

Histological images were taken with a Nikon Eclipse E3800 microscope (Melville, NY) using a digital camera (QImaging Inc., Surrey, Canada) and SimplePCI imaging software version 5.3.1. Composite images were stitched together using Microsoft Image Composite Editor v1.4.4 (Microsoft Corporation, Redmond, WA).

4.3 Results

Fluoride significantly upregulated ferroportin (Fpn) expression

To examine the association of reduced pigmentation and interference of iron transport, I measured the expression and synthesis of two proteins functioning for iron import (transferrin receptor, TFRC) and iron export (ferroportin, FPN). Mandibular incisors of mice given 0 or 50 ppm F in drinking water were immunostained for transferrin receptor (TFRC), iron importing protein. When fluoride-exposed maturation ameloblasts were compared to controls, no apparent differences were seen (Figure 16A). I was unable to immunodetect iron-exporting protein ferroportin (FPN).

I examined mRNA expression of *Tfrc* and *Fpn* in maturation ameloblasts to determine if fluoride affected expression. While fluoride did not significantly change expression of *Tfrc*, I found a highly significant increase in *Fpn* mRNA expression (Figure 16B).

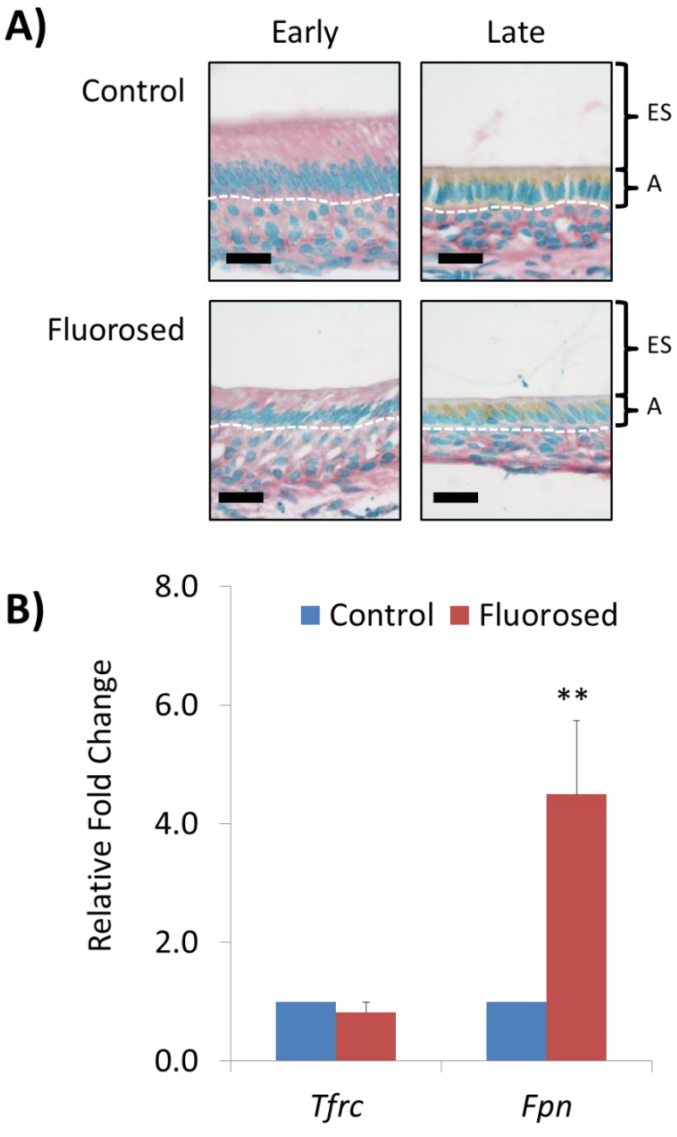

Figure 16 *Fluoride significantly upregulated ferroportin (Fpn) expression without affecting expression or synthesis of transferrin receptor (Tfrc).*
(A) Images of early- and late-stage maturation ameloblasts stained with anti-TFRC and methyl green counterstain from mice given 0 or 50 ppm F in drinking water showed no change in TFRC immunostaining in fluoride exposed ameloblasts. 25µm scale bar (E) Similarly, relative fold change of *Tfrc* and *Fpn* expression from maturation-stage enamel organs harvested from control and fluorosed mice showed a significant increase in expression of *Fpn* in fluoride exposed mice. Fold change was calculated relative to the baseline expression of the gene in control mice. Genes were normalized to the expression of Mrpl19 (mouse ribosomal protein L19). ** $p < 0.01$
Abbreviations: ES – enamel space, A – maturation ameloblasts

Fluoride does not obviously change Fe^{3+} storage as measured by Prussian blue staining, but decreases expression and synthesis heavy chain ferritin (Fth)

Because I found fluoride altered expression of *Fpn*, I further investigated the possibility that iron accumulation in maturation ameloblasts was altered. To examine this possibility, I used Prussian blue staining to determine if fluoride altered ferric (Fe^{3+}) iron levels in maturation ameloblasts. When fluoride-exposed maturation ameloblasts were compared to controls, no apparent differences were seen (Fig 17A-D). There were no obvious effects on the synthesis of light chain subunit of the iron-storage protein ferritin (FTL) (Fig 17E-H). However, immunostaining for the heavy chain subunit of ferritin (FTH) showed evidence of decreased FTH synthesis in maturation stage ameloblasts (Fig 17I-L).

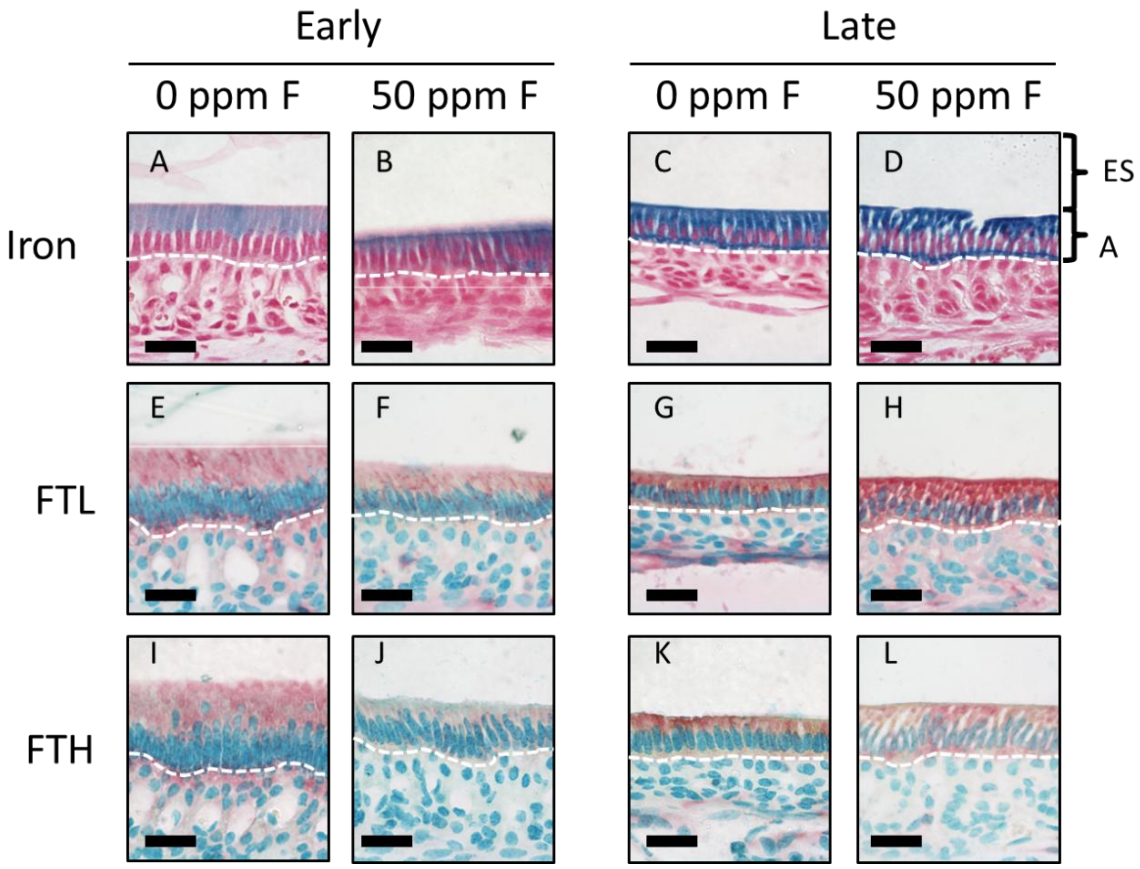

Figure 17 *Fluoride did not affect ferric iron levels in maturation ameloblasts*
(A-L) Images of early- and late-stage maturation ameloblasts stained with either Prussian blue staining for iron, followed by a with nuclear-fast red counterstain (A-D), or anti-FTL (E-H), or anti-FTH (I-L) red immunostaining with methyl green counterstain from mice given 0 or 50 ppm F in drinking water showed reduced FTH immunostaining in fluoride exposed ameloblasts. 25um scale bar
Abbreviations: ES – enamel space, A – maturation ameloblast

To examime if the decrease in FTH synthesis is a result of reduced *Fth* expression, we examined mRNA expression of *Ftl* and *Fth*. Consistent with my immunohistochemical analyses, maturation ameloblasts from fluorosed mice incisors had a significant decrease in *Fth* mRNA expression, but no change to *Ftl* (Fig 18).

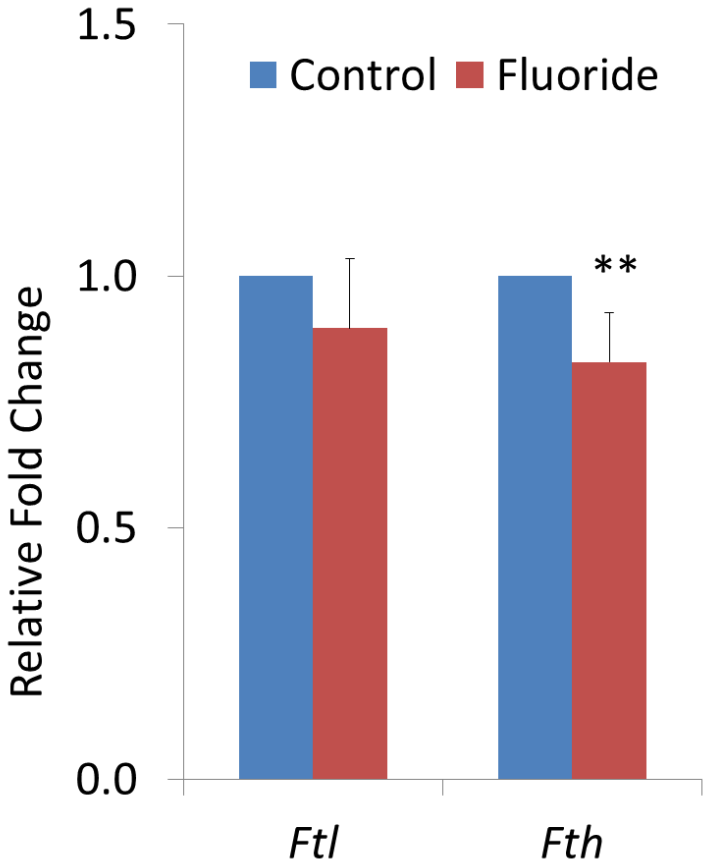

Figure 18 *Fluoride significantly affected expression of the heavy chain subunit of ferritin (Fth)*
Relative fold change of *Ftl* and *Fth* expression from maturation-stage enamel organs harvested from control and fluorosed mice showed a significant decrease in the expression of *Fth* in fluoride exposed mice. Fold change was calculated relative to the baseline expression of the gene in control mice. Genes were normalized to the expression of Mrpl19 (mouse ribosomal protein L19). ** $p < 0.01$

Fluoride increased activation of NFκB and decreased SOD1 synthesis in maturation ameloblasts

The use of Prussian blue staining to assess iron levels only detects iron found as ferric (Fe^{3+}) iron (Sheehan and Hrapchak, 1980). Iron can also exist in cells as ferrous (Fe^{2+}) iron when forming the intracellular labile iron pool (LIP) (Breuer et al., 1995). An increased LIP size is known to result in a larger LIP and increased reactive oxygen species (ROS) formation (Kakhlon et al., 2001). To address the increased formation of ROS, cells increase synthesis of enzymes like superoxide dismutase (SOD1) to convert ROS into less reactive moieties (Kruszewski, 2003). Therefore, I used SOD1 as an indicator of the relative size of LIP and intracellular Fe^{2+} levels. Immunostaining for SOD1 in early maturation ameloblasts showed fluoride exposure resulted in decreased synthesis of SOD1 (Fig 19A-B). SOD1 was not detected in late maturation ameloblasts regardless of fluoride treatment (Fig 19C-D).

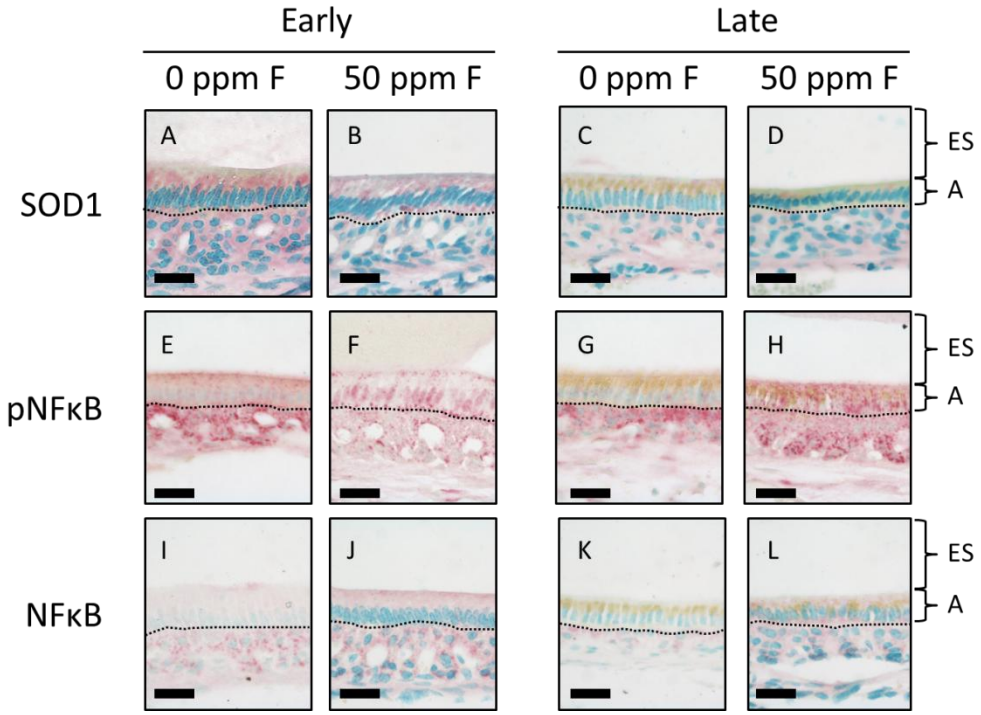

Figure 19 *Fluoride increased activation of NFκB and decreased SOD1 synthesis in maturation ameloblasts*
Images of early- and late-stage maturation ameloblasts stained with anti-SOD1 (A-D), anti-NFκB (E-H), or anti-p-NFκB (I-L) red immunostaining with methyl green counterstain from mice given 0 or 50 ppm F in drinking water. Though there were changes immunostaining of SOD1and NFκB in early maturation stage ameloblasts, there were no obvious changes at late maturation, when peak iron accumulation was observed in ameloblasts.
Abbreviations: ES – enamel space, A – maturation ameloblast,

NFκB is known to regulate iron storage by stimulating the synthesis of FTH (Pham et al., 2004). I assessed activation of NFκB (phosphorylated NFκB, pNFκB) by immunostaining. Immunostaining for pNFκB (which signifies that NFκB is transcriptionally active) showed nuclear translocation in maturation ameloblasts after fluoride exposure, indicating fluoride-related NFκB activation (Fig 19I-L). Immunostaining for total NFκB also showed fluoride increased NFκB synthesis in maturation ameloblasts when compared to controls (Figure 19E,G), which showed no obvious NFκB immunostaining (Fig 19E,G).

4.4 Discussion

Iron is an important element for many cellular processes, including cellular respiration and DNA repair (Cammack et al., 1990). Maturation ameloblasts in rodents accumulate iron during amelogenesis (Smith, 1998; Wen and Paine, 2013). This iron appears to move from the ameloblasts to the enamel surface late in maturation, leaving the surface a dark, yellow color (Wen and Paine, 2013). Although it has been reported that rats with long-term iron-deficiency had varied degrees of enamel structural abnormality, including hypoplasticity and disturbed arrangement of enamel prisms (Prime et al., 1984), the clear role of iron in rodent teeth is not known. Some authors have suggested that iron enhances wear and acid resistance of the enamel (Dumont et al., 2014; Kato et al., 1988). Because it has been reported that rodents exposed to high fluoride levels results in enamel with decreased acid resistance and less pigmentation in enamel (Everett et al., 2002; Saiani et al., 2009), we explored mechanisms to regulate the formation of iron pigmentation using fluorosed mice model. First of all, I tried to determine if fluoride affected the ability of ameloblasts to import or export iron. I found that fluoride did not change the expression and synthesis of TFRC, this suggests fluoride does not affect the ability of ameloblasts to import iron during maturation stage.

When investigating iron export, ferroportin (FPN) is the only known protein that exports iron out of cells (Ward and Kaplan, 2012). Although I was not successful immunostaining for FPN in MAB, it was surprising to see fluoride significantly upregulating *Fpn* expression, suggesting that fluoride-exposed ameloblasts have increased the ability to export iron. It is not clear the consequence of this upregulated *Fpn* expression on iron pigmentation and intracellular iron levels, nor how fluoride results in increased *Fpn* expression maturation ameloblasts. One explanation is fluoride increases intracellular zinc (Zn^{2+}) concentration through changes in the metal ion transport dynamics of divalent metal transporter-1 (DMT-1), as it is hypothesized that fluoride may have an effect on transport dynamics of DMT-1 to promote the increased concentration of zinc like it does for lead (Pb^{2+}) in calcified tissues (Sawan et al., 2010). The increase in zinc influx would not only inhibit iron uptake (Iyengar et al., 2009), but also activate metal-responsive transcription factor-1 (MTF-1), which is known to upregulate *Fpn* expression (Troadec

et al., 2010). Thus, additional studies are needed to determine the impact of fluoride-related changes on iron export on iron pigmentation.

Furthermore, because of the significant upregulation of *Fpn* expression, I wanted to assess if intracellular iron levels were altered. Prussian blue staining, which transforms ferric (Fe^{3+}) iron into a blue color pigment, revealed fluoride may not affect levels of Fe^{3+} iron within ameloblasts. To confirm that the capacity of maturation ameloblasts to store Fe^{3+} iron intracellular was not affected, I checked expression and synthesis of light (FTL) and heavy chain (FTH) subunits of ferritin. While FTL was not affected by fluoride, fluoride did decrease both *Fth* expression and FTH synthesis. The ratio of FTH and FTL subunits in ferritin can vary in different cell types (Cairo et al., 1991), and only FTH has ferroxidase activity necessary to allow ferrous (Fe^{2+}) iron to be mineralized and stored by FTL within ferritin as Fe^{3+} iron. LIP size can change based on the expression levels of the *Ftl* and *Fth* (Kakhlon et al., 2001). If FTH is downregulated, an increase in Fe^{2+} levels could be expected as there is less FTH to provide Fe^{3+} used by FTL. In general, LIP size is carefully managed to control intracellular levels of reactive oxygen species (ROS), which can damage nucleic acid, proteins, and lipids to negative cellular function (Ray et al., 2012). This implies increases in LIP size should result in increased ROS levels. A cell with a larger LIP would increase synthesis of enzymes like SOD1 to keep ROS levels in check as these enzymes would transform the ROS into something less reactive.

Directly evaluating intracellular levels of Fe^{2+} iron *in vivo* is challenging because of its highly reactive nature compared to Fe^{3+} iron (Spangler et al., 2016). Thus, I had to use indirect approaches to evaluate LIP size by detecting SOD1. It was unexpected that SOD1 synthesis decreased as a result. However, my findings confirm another study which found *in vitro* exposure of murine first molar germs to millimolar levels of fluoride decreases SOD1 synthesis (Jacinto-Aleman et al., 2010). However, SOD1 is not the only enzyme that ameliorates ROS, as there is also catalase and glutathione synthase (Lu, 2013; Nguyen Ngoc et al., 2012). Therefore, additional examination of those enzymes is necessary to conclude the decrease of Fe^{2+} level in the fluorosed maturation ameloblasts.

Furthermore, the decreased FTH protein synthesis and mRNA expression also indicates the lowered intracellular Fe^{2+} iron. Anderson et al. has reported that the high levels of free intracellular iron promote expression of *Fth,* as the iron binds competitively to iron-regulatory protein 1 (IRP1), preventing IRP1 binding to *Fth* mRNA and promoting degradation of *Fth* mRNA (Anderson et al., 2012). Thus, lower free iron (i.e. intracellular Fe^{2+}) would result in the reduced *Fth* expression.

Cells have many sensors to detect when ROS levels are increasing. Cells counter the increase in ROS formation through a three-pronged response: (1) reducing catalysis for ROS formation (e.g. unbound iron), (2) increasing production of enzymes like superoxide dismutase 1 (SOD1) to ameliorate free radicals, and (3) upregulating biomolecule repair pathways. One of these mechanisms includes nuclear factor kappa-light-chain-enhancer of activated B cells (NFκB), a transcription factor associated with the antioxidant response, which is often activated in the presence of ROS (Schreck et al., 1991). NFκB activation by ROS upregulates *Fth* mRNA expression (Pham et al., 2004). However, my findings showed increased activation of NFκB in the fluorosed maturation ameloblasts, but decreased SOD1 synthesis and reduced *Fth* expression. It could also be that intracellular iron levels is a more potent regulator of *Fth* mRNA expression than NFκB as *Fth* mRNA expression is regulated post-transcriptionally by iron. In addition, my finding of the decreased synthesis of SOD1 by fluoride could suggest that maturation ameloblasts do not experience high levels of ROS when exposed to fluoride, suggesting NFκB is not being activated by ROS.

Furthermore, NFκB-induced transcription of *Sod1* may require activation of that phosphatidylinositol 3 kinase (PI3K) pathway (Rojo et al., 2004). It has been reported that exposure to high levels of fluoride did not alter phosphorylation levels of PI3K in ovarian tissues despite the increase detected ROS levels (Geng et al., 2014). Thus, further studies are needed to confirm the possibility that fluoride interferes with activation of the PI3K pathway in maturation ameloblasts.

Though the role of iron in maturation ameloblasts remains to be understood, these studies suggest that

either iron is released from the ameloblasts when matrix mineralization is nearly complete, or perhaps when mineralization is almost complete, the iron is no longer incorporated into the enamel matrix, but remains on the surface. This possibility is consistent with the general lack of iron pigmentation in all forms of amelogenesis imperfecta in rodent incisors. $Klk4^{-/-}$, $Fam20C^{-/-}$, $Enam^{-/-}$, and $AmelX^{-/-}$ mice lack pigmentation in their incisors as compared to wildtype controls (Gibson et al., 2001b; Masuya et al., 2005; Simmer et al., 2009; Wang et al., 2012). A study analyzing the composition of acid susceptible human dental enamel (as determined by formation of white spot lesions ex-vivo) found such enamel had lower calcium phosphate to organic material ratio as compared to acid resistant enamel. (Besic et al., 1975). Furthermore, the same study showed the average concentration of iron in acid susceptible enamel (492 ppm) was approximately half of the concentration of the acid-resistant enamel (1075 ppm) and iron was detected up to 300 um into the enamel of both groups. These findings suggest that iron deposition is a normal part amelogenesis and the amount of iron deposited into the enamel influences its ability to resist acid.

In summary, high exposure to fluoride during amelogenesis may result in decreased intracellular iron levels to impact iron deposition in to dental enamel.

Chapter 5
Summary and Future Directions

In this dissertation, I explored the many mechanisms that regulate ameloblast differentiation and function during amelogenesis.

I investigated the function of amelogenins on driving ameloblast differentiation. It was long assumed that secretion of the amelogenin-rich enamel matrix was instrumental of enabling ameloblasts to transition their cellular programming from matrix secretion to matrix resorption and mineralization. While I discovered that miRNA derived from alternative splicing of exon 4 from the amelogenin gene contributes to the programming of secretory ameloblasts, its role in maturation stage still needs to be elucidated. Because altering expression of any miRNA would impact the regulation of hundreds of genes, it would be interesting to explore any effects of fluoride on miRNA expression to produce the varied effects we see in the severity of dental fluorosis.

In maturation ameloblasts, I identified that androgen receptor (AR) signaling is present and has a role in in *Klk4* expression. This result was found by using a rodent fluorosis model, where I showed that fluoride exposure results in ameloblasts having reduced AR translocation that is mediated through changes in TGF-β signaling. This discovery has three profound implications. The first is that I am the first to demonstrate the involvement of steroid hormones and steroid signaling for amelogenesis. Development of teeth is affected by gender just like development of other tissues like the brain. The second is association of AR signaling of being an *intracellular* regulator of key genes related to amelogenesis. While many extracellular signaling pathways have been identified to be important in amelogenesis, such as TGF-β signaling, it has been long unknown what provided direct regulation of key amelogenesis-related genes. While AR signaling is still an indirect regulator of *Klk4* expression, my work has narrowed the list of what factors are needed to produce *Klk4* expression during maturation stage amelogenesis. The last implication is the confirmation that fluoride affects AR signaling. Because AR signaling is important in

the function of many other tissues, such as in the prostate and testis, additional explorations are needed to determine the impact every day exposure to fluoride on AR signaling in the function of such tissues.

Lastly, I explored the transport of iron in maturation ameloblasts. While fluoride did not appear to directly affect iron storage in ferritin, my studies suggest that fluoride alters Fe^{2+} iron transport out of ameloblasts. While my findings suggested that fluoride resulted in maturation ameloblasts having decreased need for enzymes like SOD1 to ameliorate ROS, I found fluoride activated NFκB, which would normally upregulate *Sod1* expression if there were increased ROS. Thus, future studies to determine if fluoride alters Fe^{2+} levels should use more direct approaches to determine the relationship between iron and maturation ameloblast differentiation.

A larger question that still remains is how ameloblasts sense when to transition its cellular programming throughout the various stages of amelogenesis. Understanding how the ameloblasts properly time its transitions from one program to another would open insights in how subtle differences in gene expression affect enamel in its quality and susceptibility to dental caries. These subtle differences that cannot be macroscopically seen in dental enamel may have a profound influence in the ability of people to in prevent the development of dental caries in their teeth. Thus, knowing which populations who are at increased risk would permit the more efficient use of limited resources to decrease the incidence of dental caries around the world.

References

Adeyemi TA, Isiekwe MC. 2003. Comparing permanent tooth sizes (mesio-distal) of males and females in a Nigerian population. West African journal of medicine 22(3):219-221.

Ahrens-Fath I, Politz O, Geserick C, Haendler B. 2005. Androgen receptor function is modulated by the tissue-specific AR45 variant. Febs J 272(1):74-84.

Anderson CP, Shen M, Eisenstein RS, Leibold EA. 2012. Mammalian iron metabolism and its control by iron regulatory proteins. Biochim Biophys Acta 1823(9):1468-1483.

Aoba T. 1997. The effect of fluoride on apatite structure and growth. Crit Rev Oral Biol Med 8(2):136-153.

Auyeung VC, Ulitsky I, McGeary SE, Bartel DP. 2013. Beyond secondary structure: primary-sequence determinants license pri-miRNA hairpins for processing. Cell 152(4):844-858.

Bansal K, Goyal M, Dhingra R. 2016. Association of severe early childhood caries with iron deficiency anemia. Journal of the Indian Society of Pedodontics and Preventive Dentistry 34(1):36-42.

Bartel DP. 2004. MicroRNAs: genomics, biogenesis, mechanism, and function. Cell 116(2):281-297.

Bartel DP. 2009. MicroRNAs: target recognition and regulatory functions. Cell 136(2):215-233.

Benjamini Y, Hochberg Y. 1995. Controlling the false discovery rate: a practical and powerful approach to multiple testing. Journal of the Royal Statistical Society Series B (Methodological):289-300.

Berkovitz BK, Heap PF. 1976. The effect of fluoride on iron, calcium and phosphorus distribution in the rat incisor. Caries Res 10(5):337-351.

Besic FC, Bayard M, Wiemann MR, Jr., Burrell KH. 1975. Composition and structure of dental enamel: elemental composition and crystalline structure of dental enamel as they relate to its solubility. J Am Dent Assoc 91(3):594-601.

Breuer W, Epsztejn S, Cabantchik ZI. 1995. Iron acquired from transferrin by K562 cells is delivered into a cytoplasmic pool of chelatable iron(II). J Biol Chem 270(41):24209-24215.

Bronckers AL, Engelse MA, Cavender A, Gaikwad J, D'Souza RN. 2001. Cell-specific patterns of Cbfa1 mRNA and protein expression in postnatal murine dental tissues. Mechanisms of development 101(1-2):255-258.

Bronckers AL, Lyaruu D, Jalali R, Medina JF, Zandieh-Doulabi B, DenBesten PK. 2015. Ameloblast Modulation and Transport of Cl(-), Na(+), and K(+) during Amelogenesis. J Dent Res 94(12):1740-1747.

Cairo G, Rappocciolo E, Tacchini L, Schiaffonati L. 1991. Expression of the genes for the ferritin H and L subunits in rat liver and heart. Evidence for tissue-specific regulations at pre- and post-translational levels. Biochem J 275 (Pt 3):813-816.

Cammack R, Wrigglesworth JM, Baum H. 1990. Iron-dependent enzymes in mammalian systems. In: Ponka PS, H.M., Woodworth RC, editors. Iron Transport and Storage. Cleveland, OH: CRC Press. p 17-39.

Cho A, Haruyama N, Hall B, Danton MJ, Zhang L, Arany P, Mooney DJ, Harichane Y, Goldberg M, Gibson CW, Kulkarni AB. 2013. TGF-B Regulates Enamel Mineralization and Maturation through KLK4 Expression. PLoS One 8(11):e82267.

Cho ES, Kim KJ, Lee KE, Lee EJ, Yun CY, Lee MJ, Shin TJ, Hyun HK, Kim YJ, Lee SH, Jung HS, Lee ZH, Kim JW. 2014. Alteration of conserved alternative splicing in AMELX causes enamel defects. J Dent Res 93(10):980-987.

Clark RB. 1977. Nephrotoxic levels of fluoride. Anesthesia and analgesia 56(6):877.

Coffield KD, Phillips C, Brady M, Roberts MW, Strauss RP, Wright JT. 2005. The psychosocial impact of developmental dental defects in people with hereditary amelogenesis imperfecta. J Am Dent Assoc 136(5):620-630.

Comstock CE, Augello MA, Schiewer MJ, Karch J, Burd CJ, Ertel A, Knudsen ES, Jessen WJ, Aronow BJ, Knudsen KE. 2011. Cyclin D1 is a selective modifier of androgen-dependent signaling and androgen receptor function. J Biol Chem 286(10):8117-8127.

Den Besten PK. 1986. Effects of fluoride on protein secretion and removal during enamel development in the rat. J Dent Res 65(10):1272-1277.
Denbesten P, Li W. 2011. Chronic fluoride toxicity: dental fluorosis. Monogr Oral Sci 22:81-96.
DenBesten PK, Crenshaw MA, Wilson MH. 1985. Changes in the fluoride-induced modulation of maturation stage ameloblasts of rats. J Dent Res 64(12):1365-1370.
DenBesten PK, Yan Y, Featherstone JD, Hilton JF, Smith CE, Li W. 2002. Effects of fluoride on rat dental enamel matrix proteinases. Arch Oral Biol 47(11):763-770.
Dodgen H, Rollefson G. 1949. The complex ions formed by iron and thorium with fluoride in acid solution. J Am Chem Soc 71(8):2600-2607.
Dumont M, Tutken T, Kostka A, Duarte MJ, Borodin S. 2014. Structural and functional characterization of enamel pigmentation in shrews. J Struct Biol 186(1):38-48.
El Hage Chahine JM, Hemadi M, Ha-Duong NT. 2011. Uptake and release of metal ions by transferrin and interaction with receptor 1. Biochim Biophys Acta.
Everett ET, McHenry MA, Reynolds N, Eggertsson H, Sullivan J, Kantmann C, Martinez-Mier EA, Warrick JM, Stookey GK. 2002. Dental fluorosis: variability among different inbred mouse strains. J Dent Res 81(11):794-798.
Everett ET, Yan D, Weaver M, Liu L, Foroud T, Martinez-Mier EA. 2009. Detection of dental fluorosis-associated quantitative trait Loci on mouse chromosomes 2 and 11. Cells Tissues Organs 189(1-4):212-218.
Fan Y, Zhou Y, Zhou X, Sun F, Gao B, Wan M, Zhou X, Sun J, Xu X, Cheng L, Crane J, Zheng L. 2015. MicroRNA 224 Regulates Ion Transporter Expression in Ameloblasts To Coordinate Enamel Mineralization. Mol Cell Biol 35(16):2875-2890.
Fukumoto S, Nakamura T, Yamada A, Arakaki M, Saito K, Xu J, Fukumoto E, Yamada Y. 2014. New insights into the functions of enamel matrices in calcified tissues. Japanese Dental Science Review 50(2):47-54.
Geng Y, Qiu Y, Liu X, Chen X, Ding Y, Liu S, Zhao Y, Gao R, Wang Y, He J. 2014. Sodium fluoride activates ERK and JNK via induction of oxidative stress to promote apoptosis and impairs ovarian function in rats. Journal of hazardous materials 272:75-82.
Gibson CW, Yuan ZA, Hall B, Longenecker G, Chen E, Thyagarajan T, Sreenath T, Wright JT, Decker S, Piddington R, Harrison G, Kulkarni AB. 2001a. Amelogenin-deficient mice display an amelogenesis imperfecta phenotype. The Journal of biological chemistry 276(34):31871-31875.
Gibson CW, Yuan ZA, Hall B, Longenecker G, Chen E, Thyagarajan T, Sreenath T, Wright JT, Decker S, Piddington R, Harrison G, Kulkarni AB. 2001b. Amelogenin-deficient mice display an amelogenesis imperfecta phenotype. J Biol Chem 276(34):31871-31875.
Guy W S, Taves D R, Brey W S. 1976. Organic Fluorocompounds in Human Plasma: Prevalence and Characterization. Biochemistry Involving Carbon-Fluorine Bonds: AMERICAN CHEMICAL SOCIETY. p 117-134.
Halse A. 1972a. An electron microprobe investigation of the distribution of iron in rat incisor enamel. Scand J Dent Res 80(1):26-39.
Halse A. 1972b. Location and first appearance of rat incisor pigmentation. Scand J Dent Res 80(5):428-433.
Halse A. 1973. Effect of dietary iron deficiency on the pigmentation and iron content of rat incisor enamel. Scand J Dent Res 81(4):319-334.
Halse A, Selvig KA. 1974. Incorporation of iron in rat incisor enamel. Scand J Dent Res 82(1):47-56.
He WW, Kumar MV, Tindall DJ. 1991. A frame-shift mutation in the androgen receptor gene causes complete androgen insensitivity in the testicular-feminized mouse. Nucleic Acids Res 19(9):2373-2378.
Hu JC, Chun YH, Al Hazzazzi T, Simmer JP. 2007. Enamel formation and amelogenesis imperfecta. Cells Tissues Organs 186(1):78-85.
Hu JC, Sun X, Zhang C, Liu S, Bartlett JD, Simmer JP. 2002. Enamelysin and kallikrein-4 mRNA expression in developing mouse molars. Eur J Oral Sci 110(4):307-315.

Iyengar V, Pullakhandam R, Nair KM. 2009. Iron-zinc interaction during uptake in human intestinal Caco-2 cell line: kinetic analyses and possible mechanism. Indian journal of biochemistry & biophysics 46(4):299-306.
Jacinto-Aleman LF, Hernandez-Guerrero JC, Trejo-Solis C, Jimenez-Farfan MD, Fernandez-Presas AM. 2010. In vitro effect of sodium fluoride on antioxidative enzymes and apoptosis during murine odontogenesis. J Oral Pathol Med 39(9):709-714.
Jalali R, Guo J, Zandieh-Doulabi B, Bervoets TJ, Paine ML, Boron WF, Parker MD, Bijvelds MJ, Medina JF, DenBesten PK, Bronckers AL. 2014. NBCe1 (SLC4A4) a potential pH regulator in enamel organ cells during enamel development in the mouse. Cell Tissue Res 358(2):433-442.
Kakhlon O, Cabantchik ZI. 2002. The labile iron pool: characterization, measurement, and participation in cellular processes(1). Free Radic Biol Med 33(8):1037-1046.
Kakhlon O, Gruenbaum Y, Cabantchik ZI. 2001. Repression of ferritin expression increases the labile iron pool, oxidative stress, and short-term growth of human erythroleukemia cells. Blood 97(9):2863-2871.
Kato K, Nakagaki H, Sakakibara Y, Weatherell JA, Robinson C. 1988. The dissolution rate of enamel in acid in developing rat incisors. Arch Oral Biol 33(9):657-660.
Kim VN, Han J, Siomi MC. 2009. Biogenesis of small RNAs in animals. Nat Rev Mol Cell Biol 10(2):126-139.
Klokk TI, Kilander A, Xi Z, Waehre H, Risberg B, Danielsen HE, Saatcioglu F. 2007. Kallikrein 4 is a proliferative factor that is overexpressed in prostate cancer. Cancer Res 67(11):5221-5230.
Knudsen KE, Cavenee WK, Arden KC. 1999. D-type cyclins complex with the androgen receptor and inhibit its transcriptional transactivation ability. Cancer Res 59(10):2297-2301.
Ko TC, Sheng HM, Reisman D, Thompson EA, Beauchamp RD. 1995. Transforming growth factor-beta 1 inhibits cyclin D1 expression in intestinal epithelial cells. Oncogene 10(1):177-184.
Kruszewski M. 2003. Labile iron pool: the main determinant of cellular response to oxidative stress. Mutat Res 531(1-2):81-92.
Lai J, Myers SA, Lawrence MG, Odorico DM, Clements JA. 2009. Direct progesterone receptor and indirect androgen receptor interactions with the kallikrein-related peptidase 4 gene promoter in breast and prostate cancer. Molecular cancer research : MCR 7(1):129-141.
Lee HK, Lee DS, Ryoo HM, Park JT, Park SJ, Bae HS, Cho MI, Park JC. 2010. The odontogenic ameloblast-associated protein (ODAM) cooperates with RUNX2 and modulates enamel mineralization via regulation of MMP-20. J Cell Biochem 111(3):755-767.
Liu H, Sun JC, Zhao ZT, Zhang JM, Xu H, Li GS. 2011. Fluoride-induced oxidative stress in three-dimensional culture of OS732 cells and rats. Biol Trace Elem Res 143(1):446-456.
Livak KJ, Schmittgen TD. 2001. Analysis of Relative Gene Expression Data Using Real-Time Quantitative PCR and the 2−ΔΔCT Method. Methods 25(4):402-408.
Lombardo L, Marcon M, Arveda N, La Falce G, Tonello E, Siciliani G. 2016. Preliminary biometric analysis of mesiodistal tooth dimensions in subjects with normal occlusion. American journal of orthodontics and dentofacial orthopedics : official publication of the American Association of Orthodontists, its constituent societies, and the American Board of Orthodontics 150(1):105-115.
Lorenz R, Bernhart SH, Honer Zu Siederdissen C, Tafer H, Flamm C, Stadler PF, Hofacker IL. 2011. ViennaRNA Package 2.0. Algorithms for molecular biology : AMB 6:26.
Lu SC. 2013. Glutathione synthesis. Biochim Biophys Acta 1830(5):3143-3153.
Lu Y, Papagerakis P, Yamakoshi Y, Hu JC, Bartlett JD, Simmer JP. 2008. Functions of KLK4 and MMP-20 in dental enamel formation. Biol Chem 389(6):695-700.
Lyaruu DM, Bronckers AL, Mulder L, Mardones P, Medina JF, Kellokumpu S, Oude Elferink RP, Everts V. 2008. The anion exchanger Ae2 is required for enamel maturation in mouse teeth. Matrix Biol 27(2):119-127.
Lyaruu DM, Medina JF, Sarvide S, Bervoets TJ, Everts V, Denbesten P, Smith CE, Bronckers AL. 2014. Barrier formation: potential molecular mechanism of enamel fluorosis. J Dent Res 93(1):96-102.

Marsico A, Huska MR, Lasserre J, Hu H, Vucicevic D, Musahl A, Orom U, Vingron M. 2013. PROmiRNA: a new miRNA promoter recognition method uncovers the complex regulation of intronic miRNAs. Genome biology 14(8):R84.
Masuya H, Shimizu K, Sezutsu H, Sakuraba Y, Nagano J, Shimizu A, Fujimoto N, Kawai A, Miura I, Kaneda H, Kobayashi K, Ishijima J, Maeda T, Gondo Y, Noda T, Wakana S, Shiroishi T. 2005. Enamelin (Enam) is essential for amelogenesis: ENU-induced mouse mutants as models for different clinical subtypes of human amelogenesis imperfecta (AI). Hum Mol Genet 14(5):575-583.
McCord JM. 1998. Iron, free radicals, and oxidative injury. Semin Hematol 35(1):5-12.
Michon F, Tummers M, Kyyronen M, Frilander MJ, Thesleff I. 2010. Tooth morphogenesis and ameloblast differentiation are regulated by micro-RNAs. Dev Biol 340(2):355-368.
Mizukami Y, Okamura T, Miura T, Kimura M, Mogami K, Todoroki-Ikeda N, Kobayashi S, Matsuzaki M. 2001. Phosphorylation of proteins and apoptosis induced by c-Jun N-terminal kinase1 activation in rat cardiomyocytes by H(2)O(2) stimulation. Biochim Biophys Acta 1540(3):213-220.
Muto T, Miyoshi K, Horiguchi T, Noma T. 2012. Dissection of morphological and metabolic differentiation of ameloblasts via ectopic SP6 expression. J Med Invest 59(1-2):59-68.
Nakano Y, Beertsen W, van den Bos T, Kawamoto T, Oda K, Takano Y. 2004. Site-specific localization of two distinct phosphatases along the osteoblast plasma membrane: tissue non-specific alkaline phosphatase and plasma membrane calcium ATPase. Bone 35(5):1077-1085.
Nakata A, Kameda T, Nagai H, Ikegami K, Duan Y, Terada K, Sugiyama T. 2003. Establishment and characterization of a spontaneously immortalized mouse ameloblast-lineage cell line. Biochem Biophys Res Commun 308(4):834-839.
Nelson PS, Gan L, Ferguson C, Moss P, Gelinas R, Hood L, Wang K. 1999. Molecular cloning and characterization of prostase, an androgen-regulated serine protease with prostate-restricted expression. Proc Natl Acad Sci U S A 96(6):3114-3119.
Nguyen Ngoc TD, Son YO, Lim SS, Shi X, Kim JG, Heo JS, Choe Y, Jeon YM, Lee JC. 2012. Sodium fluoride induces apoptosis in mouse embryonic stem cells through ROS-dependent and caspase- and JNK-mediated pathways. Toxicol Appl Pharmacol 259(3):329-337.
Pham CG, Bubici C, Zazzeroni F, Papa S, Jones J, Alvarez K, Jayawardena S, De Smaele E, Cong R, Beaumont C, Torti FM, Torti SV, Franzoso G. 2004. Ferritin heavy chain upregulation by NF-kappaB inhibits TNFalpha-induced apoptosis by suppressing reactive oxygen species. Cell 119(4):529-542.
Presser LD, McRae S, Waris G. 2013. Activation of TGF-beta1 promoter by hepatitis C virus-induced AP-1 and Sp1: role of TGF-beta1 in hepatic stellate cell activation and invasion. PLoS One 8(2):e56367.
Prime SS, MacDonald DG, Noble HW, Rennie JS. 1984. Effect of prolonged iron deficiency on enamel pigmentation and tooth structure in rat incisors. Arch Oral Biol 29(11):905-909.
Ramsay AJ, Dong Y, Hunt ML, Linn M, Samaratunga H, Clements JA, Hooper JD. 2008. Kallikrein-related peptidase 4 (KLK4) initiates intracellular signaling via protease-activated receptors (PARs). KLK4 and PAR-2 are co-expressed during prostate cancer progression. J Biol Chem 283(18):12293-12304.
Ray PD, Huang BW, Tsuji Y. 2012. Reactive oxygen species (ROS) homeostasis and redox regulation in cellular signaling. Cell Signal 24(5):981-990.
Ritz C, Streibig JC. 2005. Bioassay analysis using R. Journal of Statistical Software 12(5):1-22.
Rojo AI, Salinas M, Martin D, Perona R, Cuadrado A. 2004. Regulation of Cu/Zn-superoxide dismutase expression via the phosphatidylinositol 3 kinase/Akt pathway and nuclear factor-kappaB. J Neurosci 24(33):7324-7334.
Saiani RA, Porto IM, Marcantonio Junior E, Cury JA, de Sousa FB, Gerlach RF. 2009. Morphological characterization of rat incisor fluorotic lesions. Arch Oral Biol 54(11):1008-1015.

Sasaki S, Takagi T, Suzuki M. 1991. Cyclical changes in pH in bovine developing enamel as sequential bands. Arch Oral Biol 36(3):227-231.
Sawan RM, Leite GA, Saraiva MC, Barbosa F, Jr., Tanus-Santos JE, Gerlach RF. 2010. Fluoride increases lead concentrations in whole blood and in calcified tissues from lead-exposed rats. Toxicology 271(1-2):21-26.
Schindelin J, Arganda-Carreras I, Frise E, Kaynig V, Longair M, Pietzsch T, Preibisch S, Rueden C, Saalfeld S, Schmid B, Tinevez JY, White DJ, Hartenstein V, Eliceiri K, Tomancak P, Cardona A. 2012. Fiji: an open-source platform for biological-image analysis. Nat Methods 9(7):676-682.
Schreck R, Rieber P, Baeuerle PA. 1991. Reactive oxygen intermediates as apparently widely used messengers in the activation of the NF-kappa B transcription factor and HIV-1. Embo J 10(8):2247-2258.
Schroth RJ, Levi J, Kliewer E, Friel J, Moffatt ME. 2013. Association between iron status, iron deficiency anaemia, and severe early childhood caries: a case-control study. BMC pediatrics 13:22.
Schwabe RF, Bradham CA, Uehara T, Hatano E, Bennett BL, Schoonhoven R, Brenner DA. 2003. c-Jun-N-terminal kinase drives cyclin D1 expression and proliferation during liver regeneration. Hepatology 37(4):824-832.
Selbach M, Schwanhausser B, Thierfelder N, Fang Z, Khanin R, Rajewsky N. 2008. Widespread changes in protein synthesis induced by microRNAs. Nature 455(7209):58-63.
Sheehan DC, Hrapchak BB. 1980. Theory and practice of histotechnology: Cv Mosby.
Sheng WS, Hu S, Feng A, Rock RB. 2013. Reactive Oxygen Species from Human Astrocytes Induced Functional Impairment and Oxidative Damage. Neurochem Res.
Shimizu D, Macho GA. 2008. Effect of enamel prism decussation and chemical composition on the biomechanical behavior of dental tissue: a theoretical approach to determine the loading conditions to which modern human teeth are adapted. Anat Rec (Hoboken) 291(2):175-182.
Shuhua X, Ziyou L, Ling Y, Fei W, Sun G. 2012. A Role of Fluoride on Free Radical Generation and Oxidative Stress in BV-2 Microglia Cells. Mediators of Inflammation 2012:8.
Simmer JP, Hu CC, Lau EC, Sarte P, Slavkin HC, Fincham AG. 1994. Alternative splicing of the mouse amelogenin primary RNA transcript. Calcif Tissue Int 55(4):302-310.
Simmer JP, Hu Y, Lertlam R, Yamakoshi Y, Hu JC. 2009. Hypomaturation enamel defects in Klk4 knockout/LacZ knockin mice. J Biol Chem 284(28):19110-19121.
Simmer JP, Richardson AS, Smith CE, Hu Y, Hu JC. 2011. Expression of kallikrein-related peptidase 4 in dental and non-dental tissues. Eur J Oral Sci 119 Suppl 1:226-233.
Sire JY, Huang Y, Li W, Delgado S, Goldberg M, Denbesten PK. 2012. Evolutionary story of mammalian-specific amelogenin exons 4, "4b", 8, and 9. Journal of dental research 91(1):84-89.
Smith CE. 1998. Cellular and chemical events during enamel maturation. Crit Rev Oral Biol Med 9(2):128-161.
Smith CE, Nanci A, Denbesten PK. 1993. Effects of chronic fluoride exposure on morphometric parameters defining the stages of amelogenesis and ameloblast modulation in rat incisors. The Anatomical record 237(2):243-258.
Somogyi-Ganss E, Nakayama Y, Iwasaki K, Nakano Y, Stolf D, McKee MD, Ganss B. 2012. Comparative temporospatial expression profiling of murine amelotin protein during amelogenesis. Cells Tissues Organs 195(6):535-549.
Spangler B, Morgan CW, Fontaine SD, Vander Wal MN, Chang CJ, Wells JA, Renslo AR. 2016. A reactivity-based probe of the intracellular labile ferrous iron pool. Nat Chem Biol 12(9):680-685.
Stahl J, Nakano Y, Horst J, Zhu L, Le M, Zhang Y, Liu H, Li W, Den Besten PK. 2015. Exon4 amelogenin transcripts in enamel biomineralization. J Dent Res 94(6):836-842.
Stahl J, Nakano Y, Kim SO, Gibson CW, Le T, DenBesten P. 2013. Leucine rich amelogenin peptide alters ameloblast differentiation in vivo. Matrix Biol 32(7-8):432-442.
Sturrock A, Alexander J, Lamb J, Craven CM, Kaplan J. 1990. Characterization of a transferrin-independent uptake system for iron in HeLa cells. J Biol Chem 265(6):3139-3145.

Suzuki M, Shin M, Simmer JP, Bartlett JD. 2014. Fluoride Affects Enamel Protein Content via TGF-beta1-mediated KLK4 Inhibition. J Dent Res.
Tang RS, Huang MC, Huang ST. 2013. Relationship between dental caries status and anemia in children with severe early childhood caries. The Kaohsiung journal of medical sciences 29(6):330-336.
Team RC. 2014. R: A language and environment for statistical computing. R Foundation for Statistical Computing, Vienna, Austria, 2012. ISBN 3-900051-07-0.
Troadec MB, Ward DM, Lo E, Kaplan J, De Domenico I. 2010. Induction of FPN1 transcription by MTF-1 reveals a role for ferroportin in transition metal efflux. Blood 116(22):4657-4664.
Tye CE, Antone JV, Bartlett JD. 2011. Fluoride does not inhibit enamel protease activity. J Dent Res 90(4):489-494.
Wang X, Wang S, Lu Y, Gibson MP, Liu Y, Yuan B, Feng JQ, Qin C. 2012. FAM20C plays an essential role in the formation of murine teeth. J Biol Chem 287(43):35934-35942.
Ward D, Kaplan J. 2012. Ferroportin-mediated iron transport: Expression and regulation. Biochim Biophys Acta.
Welbury RR, Shaw L. 1990. A simple technique for removal of mottling, opacities and pigmentation from enamel. Dental update 17(4):161-163.
Wen X, Cawthorn WP, MacDougald OA, Stupp SI, Snead ML, Zhou Y. 2011. The influence of Leucine-rich amelogenin peptide on MSC fate by inducing Wnt10b expression. Biomaterials 32(27):6478-6486.
Wen X, Paine ML. 2013. Iron Deposition and Ferritin Heavy Chain (Fth) Localization in Rodent Teeth. BMC Res Notes 6(1):1.
Wright JT, Chen SC, Hall KI, Yamauchi M, Bawden JW. 1996. Protein characterization of fluorosed human enamel. J Dent Res 75(12):1936-1941.
Xiaoying L, Yuguang G. Runx2 is involved in regulating amelotin promoter activity and gene expression in ameloblasts; 2013 25-28 May 2013. p 91-96.
Yanagawa T, Itoh K, Uwayama J, Shibata Y, Yamaguchi A, Sano T, Ishii T, Yoshida H, Yamamoto M. 2004. Nrf2 deficiency causes tooth decolourization due to iron transport disorder in enamel organ. Genes Cells 9(7):641-651.
Yang F, Chen Y, Shen T, Guo D, Dakhova O, Ittmann MM, Creighton CJ, Zhang Y, Dang TD, Rowley DR. 2014. Stromal TGF-beta signaling induces AR activation in prostate cancer. Oncotarget 5(21):10854-10869.
Ye L, Le TQ, Zhu L, Butcher K, Schneider RA, Li W, Besten PK. 2006. Amelogenins in human developing and mature dental pulp. J Dent Res 85(9):814-818.
Yin K, Hacia JG, Zhong Z, Paine ML. 2014. Genome-wide analysis of miRNA and mRNA transcriptomes during amelogenesis. BMC genomics 15:998.
Zhang Y, Kim JY, Horst O, Nakano Y, Zhu L, Radlanski RJ, Ho S, Den Besten PK. 2014. Fluorosed mouse ameloblasts have increased SATB1 retention and Galphaq activity. PLoS One 9(8):e103994.
Zhou Y, Zhang H, He J, Chen X, Ding Y, Wang Y, Liu X. 2013. Effects of sodium fluoride on reproductive function in female rats. Food Chem Toxicol 56:297-303.

Appendix 1
The complex regulation of Klk4 expression by TGF-β and Androgen Receptor Signaling in amelogenesis

A1.1 Introduction

I explored the possibility that fluorosis susceptibility was related to strain related effects of fluoride on ameloblast function, and sought to determine if a mice strain resistant to developing dental fluorosis would still exhibit cellular effects related to fluoride exposure. Furthermore, with the finding that androgen receptor signaling is involved with amelogenesis, it brings up questions whether gender plays a role in amelogenesis, as males and females have different levels of androgens. Thus, in this chapter, I did a few preliminary studies that explore how gender and mice strain affects regulators of *Klk4* expression.

A1.2 Methods

Animals

All animal procedures were carried out with approval by the University of California-San Francisco Institutional Animal Care and Use Committees. The experiments reported herein were conducted in compliance with the Animal Welfare Act and in accordance with the principles set forth in the National Research Council's *Guide for the Care and Use of Laboratory Animals*.

Three-week-old female Wistar rats (Jackson Laboratory, Sacramento, CA) were divided into two groups, with the groups given either deionized drinking water or deionized drinking water supplemented with 100 ppm sodium fluoride (Sigma-Aldrich, St. Louis, MO) *ad libitium* for four weeks. After six weeks, the rats were euthanized, the mandibles dissected and alveolar bone removed to allow access to separately dissected the enamel matrix and enamel organ for KLK4 activity assays, and quantitative real-time polymerase chain reaction (qPCR) of the relative expression of *Klk4* mRNA.

Three-week-old C57BL/6J mice and 129/SvImJ mice (Jackson) were divided into two groups, with the groups given either deionized drinking water or deionized drinking water supplemented with 50 ppm sodium fluoride (Sigma-Aldrich) *ad libitium* for four weeks. After four weeks, they were euthanized, and mandibles were obtained for morphology, immunohistochemical analyses, and qPCR of incisors.

Seven-week mice with impaired AR function due to lack of steroid and DNA binding domains caused by frameshift mutation (Ar^{Tfm}) (He et al., 1991) were purchased (Jackson), euthanized, and the mandibles obtained for morphology.

Immunohistochemistry

Mouse mandibles were dissected from other samples, and fixed in 4% paraformaldehyde in 0.06M sodium cacodylate buffer (pH 7.3) at 4°C for 24 hours. After decalcification in 8% EDTA (pH 7.3), samples were processed for routine paraffin embedding and sagittally sectioned. The sections were incubated with 10% swine and 5% goat sera followed by incubation with rabbit anti-human AR (1:75;

Novus Biologicals, Littleton, CO, NB100-91658), rabbit anti-mouse TGFBR2 (1:100; Santa Cruz Biotech, Santa Cruz, CA), rabbit anti-human TGFB1 (1:50; Abcam PLC, Cambridge, MA, ab92486) antibody overnight at room temperature. A biotinylated swine anti-rabbit IgG F(ab′)2 fraction (Dako, Carpinteria, CA) was used as the secondary antibody for 1 hour at room temperature incubation. Following incubation with alkaline phosphatase conjugated streptavidin (Vector Laboratories Inc., Burlingame, CA) for 30 min, immunoreactivity was visualized using a Vector® Red kit (Vector) resulting in pink/red color for positive staining. Counter-staining was performed with methyl green (Dako). Negative control was done with normal rabbit sera.

A1.3 Results

Ameloblasts of fluoride-insensitive mice strains (129/SvImJ) did not retain matrix as compared to fluoride-sensitive mice strains (C57BL/6)

C57BL/6 (C57) mice are fluoride-sensitive and exhibits signs of fluorosis (white colored, hypomineralized enamel) when exposed to excessive levels of fluoride in drinking water (Everett et al., 2002). As expected, while C57 mice had protein retained in the maturation stage enamel space, there was not a similar retention of protein in the fluoride-exposed 129/SvImJ (129) mice, which appeared similar to the non-fluoride treated controls (Figure A1).

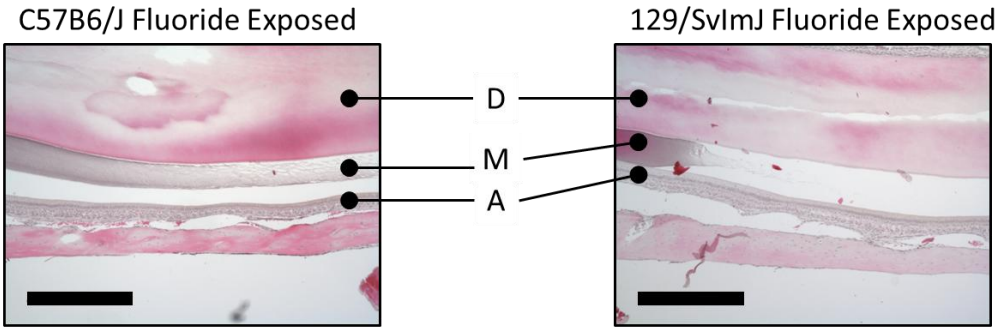

Matrix Retention	C57BL/6	129S1/SvImJ
Expected	100%	0%
Observed	100% (5/5)	0% (0/5)

Figure A1 *129/SvImJ mice do not exhibit matrix retention when exposed to fluoride*
Abbreviations: D – dentin, M –enamel matrix, A – ameloblast layer

Fluoride also reduced androgen receptor translocation in 129 mice

Because 129 mice did not exhibit matrix retention like in C57 mice when exposed to fluoride, I immunostained for AR to assess if Klk4 expression was affected. Surprisingly, fluoride reduced androgen receptor translocation in 129 mice similar to C57 mice (Figure A2).

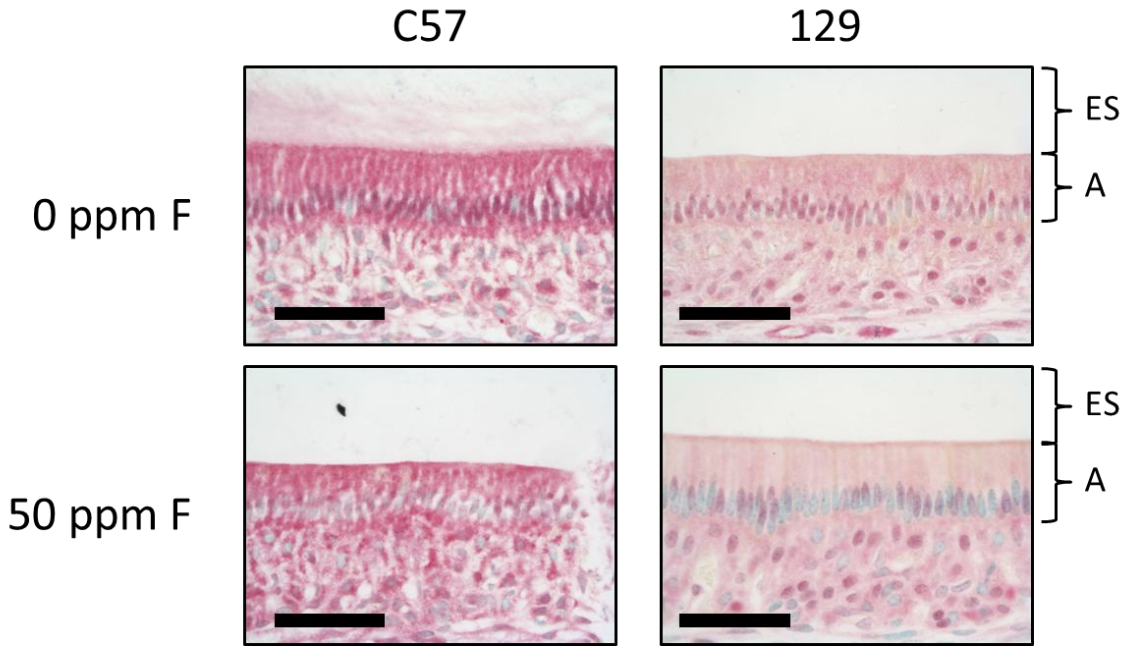

Figure A2 *Fluoride reduced androgen receptor translocation in 129 mice*
Images of maturation ameloblasts stained with either anti-AR with methyl green counterstain from mice given 0 or 50 ppm F in drinking water showed reduced. 50um scale bar
Abbreviations: ES – enamel space, A – maturation ameloblast

While fluoride reduced TGFBR2 synthesis like in C57, it increased TGFB1 synthesis in 129 mice

Because TGF-beta signaling can affect AR translocation, I immunostained for TGFBR2 and TGFB1. While TGFBR2 synthesis is decreased by fluoride in both C57 and 129 mice, TGFB1 synthesis was increased in 129 mice after fluoride exposure unlike the decreased TGFB1 synthesis seen in C57 mice (Figure A3).

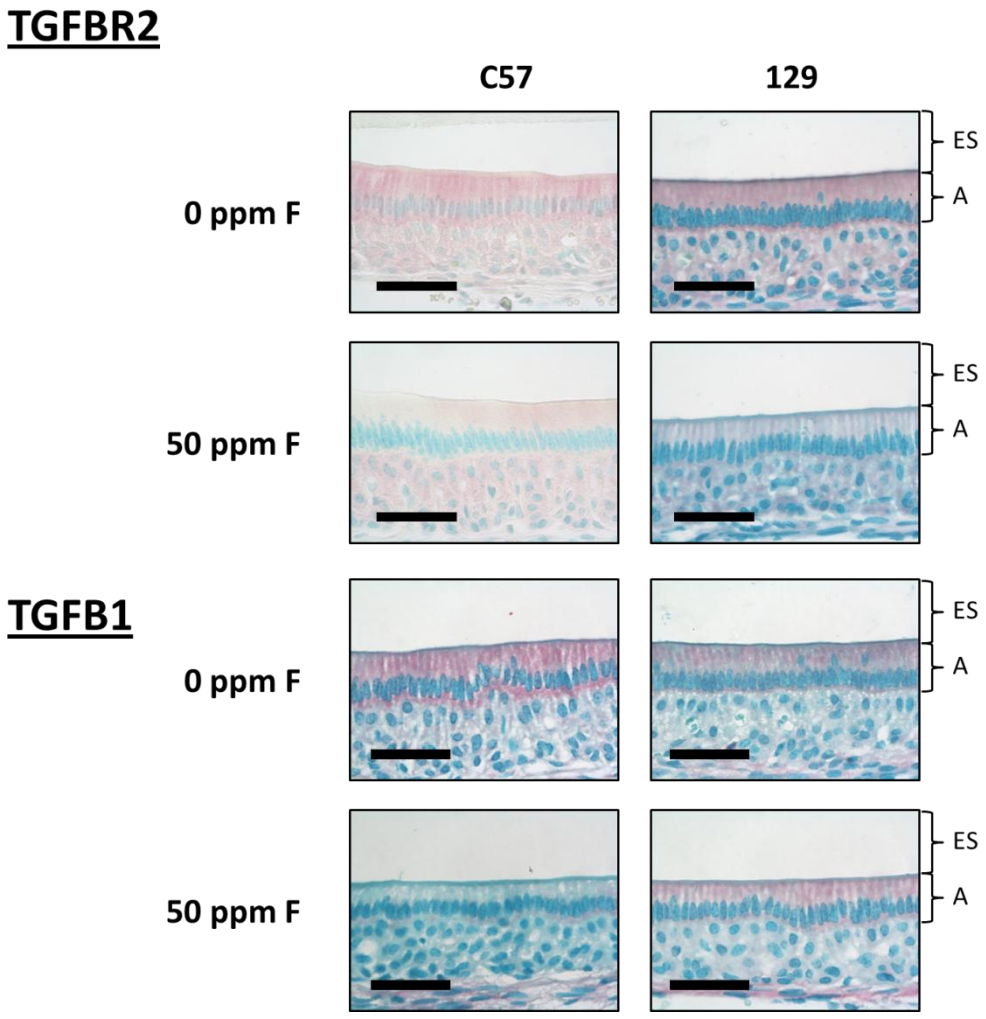

Figure A3 *While fluoride reduced TGFBR2 synthesis like in C57, it increased TGFB1 synthesis in 129 mice*
Images of maturation ameloblasts stained with either anti-TGFB2 or anti-TGFB1 with methyl green counterstain from mice given 0 or 50 ppm F in drinking water showed reduced. 50um scale bar
Abbreviations: ES – enamel space, A – maturation ameloblast

Male C57 mice have significantly reduced AR translocation, intermediate between female mice and Ar^{Tfm} where AR, though reduced, still translocated

Because of my discovery of androgen receptor involvement in *Klk4* regulation in amelogenesis, questions remain if there are differences between male and female mice in regulating *Klk4* expression. Interestingly, immunostaining of AR in male C57 mice show reduced AR translocation as compared to females (Figure A4). In chapter 2, I showed Ar^{Tfm} mice have mild enamel matrix retention as compared to female C57 mice given fluoride. Surprisingly, Ar^{Tfm} mice still exhibited androgen receptor translocation (Figure A4).

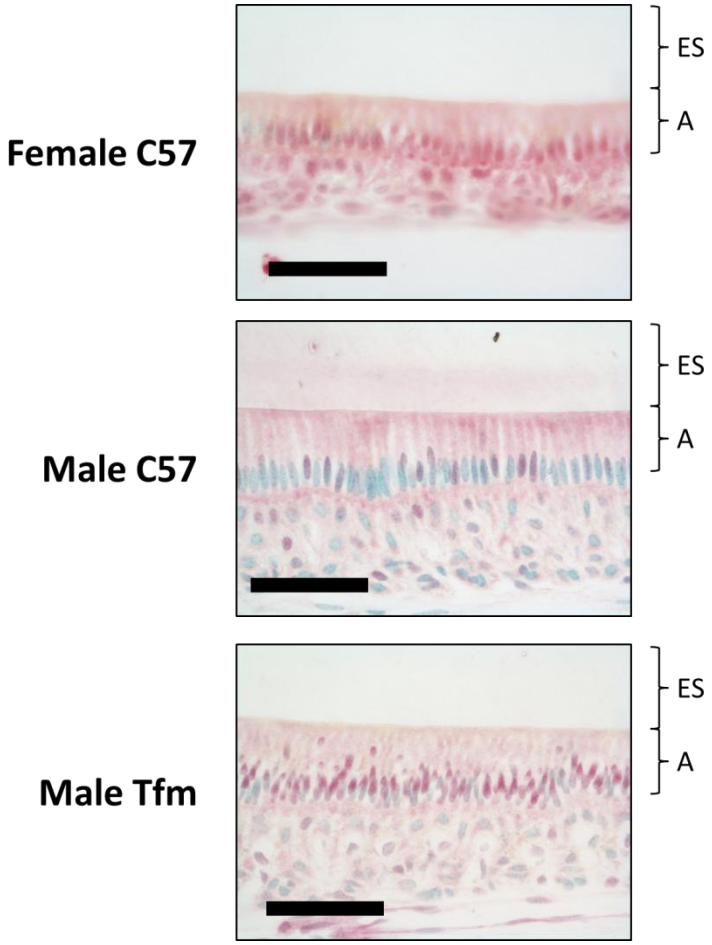

Figure A4 *While male C57 mice have significantly reduced AR translocation, Ar^{Tfm} still have AR translocation*
Images of maturation ameloblasts stained with either anti-AR with methyl green counterstain from mice given 0 or 50 ppm F in drinking water showed reduced. 50um scale bar
Abbreviations: ES – enamel space, A – maturation ameloblast

A1.4 Discussion

Many studies that strive to elucidate the mechanisms by which excessive exposure to fluoride results in dental fluorosis have often used mice strains that have been reported to be fluoride sensitive. This is the first study that extensively has used a fluoride-resistant strain to confirm cellular specific effects in fluoride-sensitive strains.

Androgen receptor has been long implicated in *Klk4* regulation in the prostate tissues, it was interesting to discover that AR receptor may play a role in *Klk4* expression during amelogenesis. Because 129 mice do not exhibit matrix retention like in C57 mice, I expected that androgen receptor translocation would not be affected. However, I did find that fluoride also affected androgen receptor translocation in 129 mice, suggesting fluoride's effect on androgen receptor translocation in ameloblasts is independent of any fluorotic changes to the enamel matrix. In addition, the degree of reduced androgen receptor translocation varied with the same concentration of fluoride exposure and correlated with the length of the maturation ameloblast layer. This suggests that reducing androgen receptor signaling may play a role in maintaining maturation ameloblast maturation stage in morphology and function, but another pathway is able to compensate for the reduced androgen receptor translocation to allow amelogenesis to still proceed despite the high levels of fluoride exposure. In this preliminary study, I did not determine whether *Klk4* mRNA expression is also reduced in 129.

I determined whether fluoride's reduction of androgen receptor translocation in female 129 mice also had reduced TGF-β signaling. I found that although there was decreased synthesis of TGFBR2, in the 129 mice there was a surprising increase in TGFB1 synthesis unlike in C57 mice. This suggests that not only is TGFB1 regulation different between C57 and 129 ameloblasts, but provides evidence that maintaining adequate TGF-B signaling may be what confers insensitivity to fluoride during amelogenesis. Furthermore, the increased TGFB1 synthesis in fluoride-exposed 129 maturation ameloblasts coincided with decreased TGFBR2 synthesis, suggesting the increase in TGFB1 synthesis is to maintain adequate TGF-β signaling.

Androgen receptor is important for proper development for both males and females, and its ligand is present at different levels depending on the age of development[1]. Because my studies have focused primarily on female mice due its ease of husbandry, it is unclear if the reduction in androgen receptor translocation is primarily due to protein inhibition of translocation (as mediated by TGF-β signaling) or reduced serum androgens present. Thus, it was surprising to see very little androgen receptor translocation in ameloblasts from male C57 mice, suggesting that males may use a different mechanism to regulate *Klk4* expression than females.

It was surprising to see positive AR translocation in Ar^{Tfm} mice. Androgen receptor gene is found on the X chromosome and is made up of 8 exons, where exon 1 codes for transcription regulation, exons 2-3 the DNA binding domain, exon 4 a hinge region, and exon 5-8 the ligand binding domain. Male mice with mutations that affect AR to bind to its ligand (required for nuclear translocation) or bind to DNA (allowing transcription of AR-regulated genes) result in Testicular feminized (Tfm) phenotype. The Ar^{Tfm} mice used in my study has a frame-shift mutation in exon 1 that results in early truncation of the protein.

However, it has been recently discovered that *Ar* gene may contain an alternative transcription start site located between in the intronic space between exon 1 and 2 called exon 1b (Ahrens-Fath et al., 2005). Transcription that starts at exon 1b would allow for formation of *Ar* mRNA to translate into an AR protein containing the key domains (like the hinge domain which the anti-AR antibody used in this study detects) needed for proper androgen receptor signaling. This could explain why the enamel matrix retention in Ar^{Tfm} incisor is quite mild compared to fluoride exposure.

[1] http://www.mayomedicallaboratories.com/test-catalog/Clinical+and+Interpretive/83686

Appendix 2
Genetic influences on fluoride's effect on ameloblast differentiation

A2.1 Introduction

Studies investigating the genetic influence on the formation of dental fluorosis have primarily focused on the enamel matrix, assessing if the canonical signs of dental fluorosis is observed in the enamel. This would suggest that anyone exposed to the same level high levels fluoride should always exhibit dental fluorosis. However, this is simply not the case because even in communities where the water would not consistently produce dental fluorosis, there are individuals who still develop dental fluorosis. The root cause of the how the dental fluorosis could be produced by any number reasons, from minor mutations in proteins such as amelogenin or KLK4 to poor physiologic management of the pH by ameloblasts to enable proper mineralization. However, there have been few studies that explore ameloblast differentiation as a contributing factor. If the timing of ameloblast differentiation changes, resulting in the shortening of the length of the maturation ameloblast layer, then we would expect amelogenesis to be incomplete when the enamel becomes exposed to the oral cavity. I used histomorphological studies and immunohistochemistry markers to explore if the timing of ameloblast differentiation is altered by fluoride.

A2.2 Methods

Section preparation

All animal procedures were carried out with approval by the University of California-San Francisco Institutional Animal Care and Use Committees. The experiments reported herein were conducted in compliance with the Animal Welfare Act and in accordance with the principles set forth in the National Research Council's *Guide for the Care and Use of Laboratory Animals*.

Three-week-old female C57BL/6J (C57) and 129/ImSvJ (129) mice were divided into two groups, with the groups given either deionized drinking water or deionized drinking water supplemented with 50 ppm sodium fluoride (Sigma-Aldrich, St. Louis, MO) *ad libitium* for four weeks. After four weeks, the mice were euthanized and the mandibles dissected out and fixed in 4% paraformaldehyde in 0.06M sodium cacodylate buffer (pH 7.3) at 4°C for 24 hours. After decalcification in 8% EDTA (pH 7.3), samples were processed for routine paraffin embedding and sagittally sectioned.

Prussian blue staining for ferric (Fe^{3+}) iron

Potassium ferrocyanide, in the presence of hydrogen chloride, reacts with ferric (Fe^{3+}) iron forms an insoluble pigment known as Prussian blue (Wen and Paine, 2013). Paraffin sections were deparaffinized, rehydrated, and immersed in a freshly prepared solution made of equal parts of 10% potassium ferrocyanide and 20% hydrochloric acid for 5 minutes. Samples were then washed with distilled water, and counterstained with nuclear fast red, dehydrated, cleared with xylene and mounted with cover slips.

Immunohistochemistry

After deparaffinization and rehydration, longitudinal mandibular incisor sections from control (0 ppm F) or fluoride-exposed (50 ppm F) were incubated with 10% swine and 5% goat sera followed by incubation with rabbit anti-FTH1 (1:200; Santa Cruz Biotech, Santa Cruz, CA) overnight at room temperature. A biotinylated swine anti-rabbit IgG F(ab′)2 fraction (Dako, Carpinteria, CA) was used as the secondary antibody for 1 h at room temperature incubation. Following incubation with alkaline phosphatase

conjugated streptavidin (Vector Laboratories Inc., Burlingame, CA) for 30 min, immunoreactivity was visualized using a Vector® Red kit (Vector) resulting in pink/red color for positive staining. Counter-staining was performed with methyl green (Dako). Negative control was done with normal rabbit sera.

Imaging

Histological images were taken with a Nikon Eclipse E3800 microscope (Melville, NY) using a digital camera (QImaging Inc., Surrey, Canada) and SimplePCI imaging software version 5.3.1. Composite images were stitched together using Microsoft Image Composite Editor v1.4.4 (Microsoft Corporation, Redmond, WA).

Measurement of the relative length of the incisor ameloblast layer

Serial sagittal sections were cut from paraffin blocks to ensure inclusion of the cervical loop and incisor alveolar bone while maximizing presence of maturation stage. These sections were used to form a composite image of the mandibular incisor. Fiji software (Laboratory for Optical and Computational Instrumentation, Madison, WI) (Schindelin et al., 2012) was used to measure histological features seen on captured composite images. The overall length of the ameloblast layer was measured staring from the cervical loop and ending where the layer was no longer encapsulated in bone.

Determine if fluoride altered various length characteristics of the ameloblast layer, the length of the ameloblast layer exhibiting maturation-stage ameloblast morphology was measured starting from the formation of the papillary layer to when yellow iron granules could not be seen within ameloblasts. The length of the ameloblast layer exhibiting positive iron-staining was measured starting from the first ameloblast exhibiting positive iron-staining to the first ameloblast with complete loss of iron-positive staining.

A2.3 Results

Fluoride resulted in the early transition of ameloblasts out of maturation stage

Muto et al. has reported that changes in maturation ameloblast differentiation in rats can result in incisors that lack pigmentation (Muto et al., 2012). Morphological observation of serial images of maturation ameloblasts along the length of the incisors from mice given 0 or 50 ppm F showed maturation ameloblasts transitioned into reduced ameloblasts (post-maturation stage) earlier in fluorosed mice compared to controls (Fig A5). The early shortening of maturation stage ameloblasts coincided with an earlier termination of iron staining and FTH immunostaining (Figure A6). However, the change in the early termination of maturation was also observed in the enamel fluorosis resistant strain 129/SvImJ (Fig A7), which did not lose iron pigmentation in its incisor even after exposure to similar levels of fluoride (Fig A8).

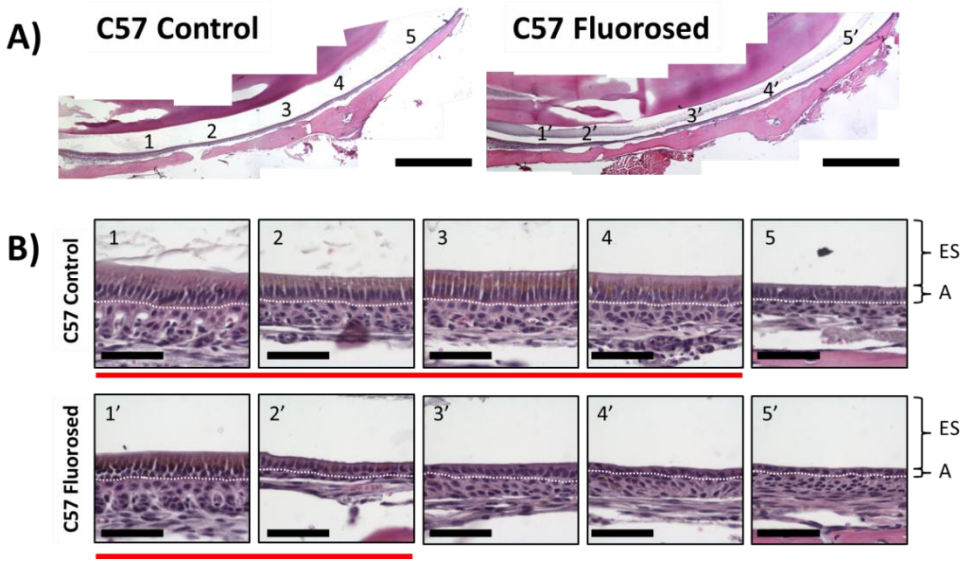

Figure A5 *Fluoride can induce maturation ameloblasts to have an early shortening morphology in C57BL/6 mice*
(A) Composite images of hematoxylin and eosin-stained mandibular incisors from mice given 0 (control) or 50 ppm F (fluorosed) in drinking water. Scale bar 500µm (B) Images labeled according to the area they were taken as represented in the top figures show when the maturation ameloblasts layer shortens in length (after red line). White line separates ameloblasts from supporting cells. Scale bar 50µm
Abbreviations: ES – enamel space, A – maturation ameloblast

Figure A6 (next page) *Detection of iron and heavy chain ferritin (FTH) synthesis correlates with maturation ameloblast layer length*
(A) Composite images of mandibular incisors from mice given 0 (control) or 50 ppm F (fluorosed) in drinking water stained with either Prussian blue staining (using nuclear fast red counterstain) or anti-FTH red immunostaining (using methyl green counterstain). Both stainings show an earlier end to staining, consistent with the early shortening of ameloblasts. Scale bar 500µm (B) Images were taken at the positions denoted in (A) composite images of mandibular incisor. The red line represents the range of ameloblasts with maturation (elongated columnar) morphology. Scale bar 50µm
Abbreviations: ES – enamel space, A – maturation ameloblast

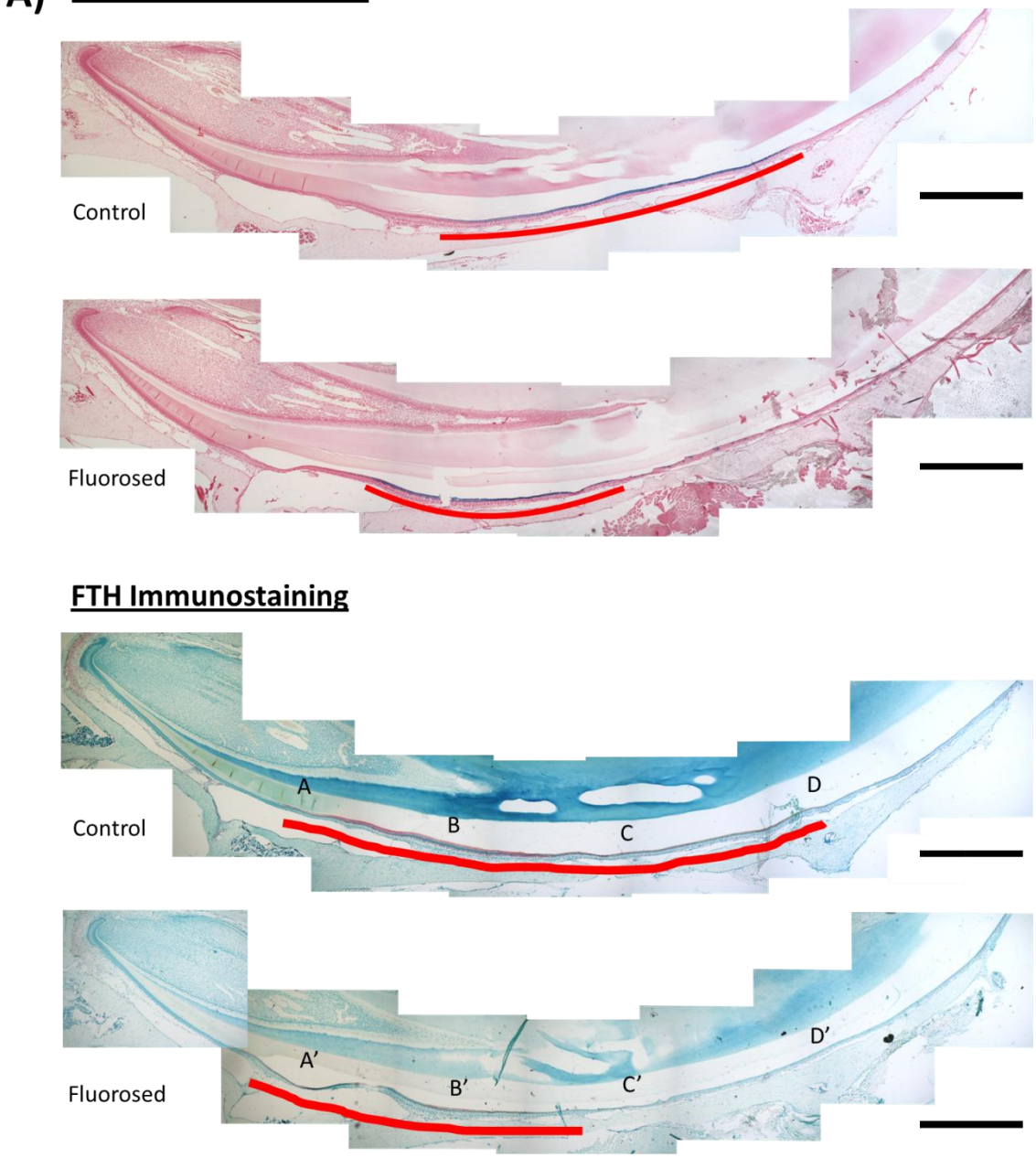
A)
Prussian Blue Staining
Control
Fluorosed
FTH Immunostaining
Control
A
B
C
D
Fluorosed
A'
B'
C'
D'
B)
Control
Fluorosed
A
B
C
D
A'
B'
C'
D'
ES
A

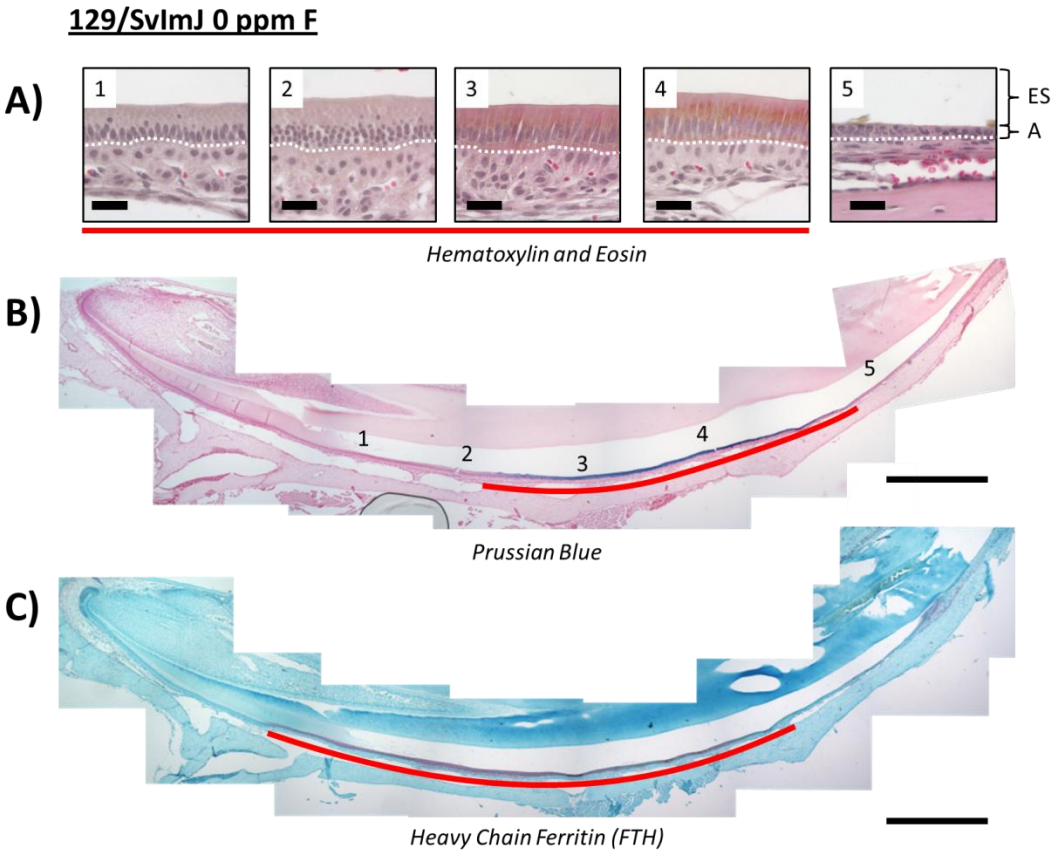
129/SvImJ 0 ppm F
A)
1
2
3
4
5
ES
A
Hematoxylin and Eosin
B)
1
2
3
4
5
Prussian Blue
C)
Heavy Chain Ferritin (FTH)
129/SvImJ 50 ppm F
D)
1
2
3
4
5
ES
A
Hematoxylin and Eosin
E)
1
2
3
4
5
Prussian Blue
F)
Heavy Chain Ferritin (FTH)

Figure A7 (previous page) *129/SvImJ can exhibit a shortened maturation ameloblast layer when exposed to fluoride*
(A, D) Images of hematoxylin and eosin-stained mandibular incisors from 129/SvImJ mice given 0 (control) or 50 ppm F in drinking water were taken at the positions denoted in (B,E) composite images of mandibular incisor. The red line represents the range of ameloblasts with maturation (elongated columnar) morphology. While line represents separation of maturation ameloblasts from supporting cells. Scale bar 25µm
Abbreviations: ES – enamel space, A – maturation ameloblasts.

(B-C, E-F) Composite images of mandibular incisors from 129/SvImJ mice given 0 (control) or 50 ppm F (fluorosed) in drinking water stained with either Prussian blue staining (using nuclear fast red counterstain) (B,E) or anti-FTH red immunostaining (using methyl green counterstain) (C, F). Both stainings show an earlier end to staining, consistent with the early shortening of maturation ameloblast layer. Scale bar 500µm

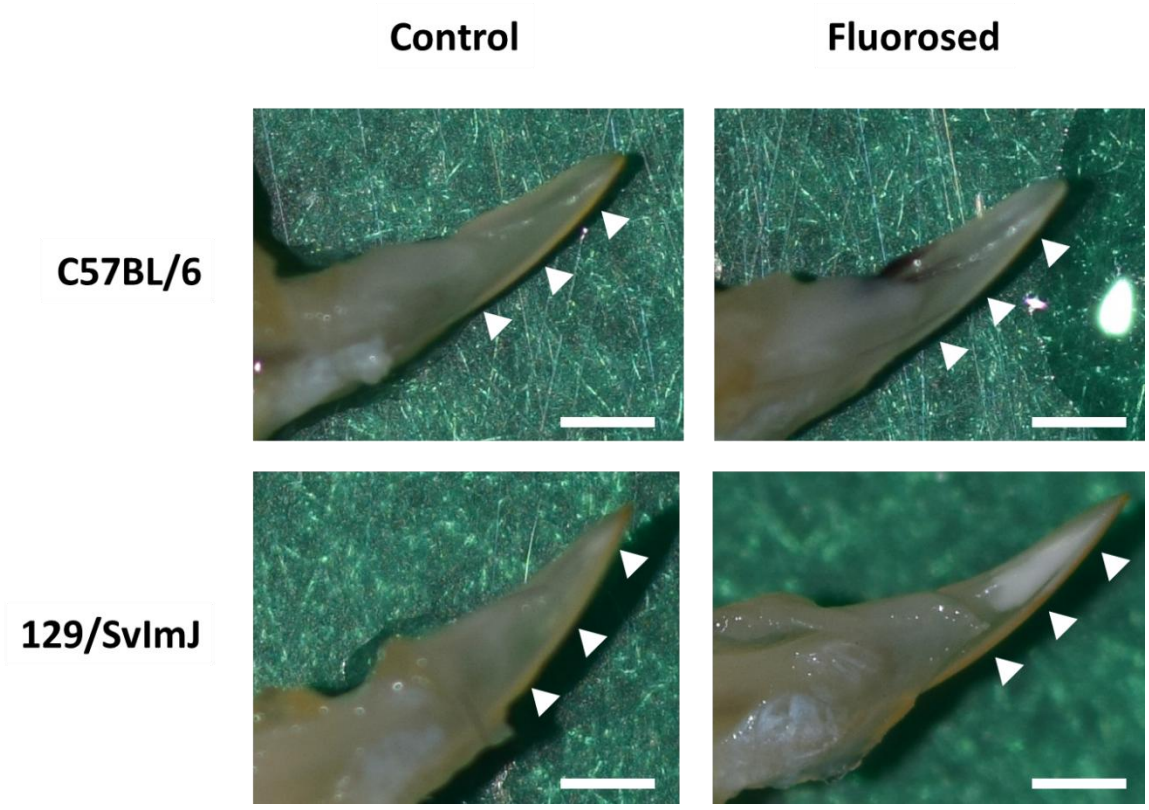

Figure A8 Exposure to *50 ppm F did not affect incisor pigmentation in 129/SvImJ mice*
Representative sagittal photographs of mandibular incisors from C57BL/6 and 129/SvImJ mice. When exposed to 50 ppm F, C57BL/6 lost incisor pigmentation (appears white) while 129/SvImJ retained incisor pigmentation (appears brown). Triangles mark incisor surface where pigmentation occurs. Scale bar 2mm.

The effects of fluoride on ameloblast differentiation were variable

The unerupted incisors had similar lengths in control and fluoride groups (Figure A9A). However, the relative number of columnar maturation stage ameloblasts (total length of ameloblasts layer on the enamel surface) was more variable in fluoride-exposed mice or both strains (Figure A9B). Greater variation was also seen in the length of the ameloblast layer that stained positive for iron in both strains of mice given fluoride as compared to control mice (Figure A9C).

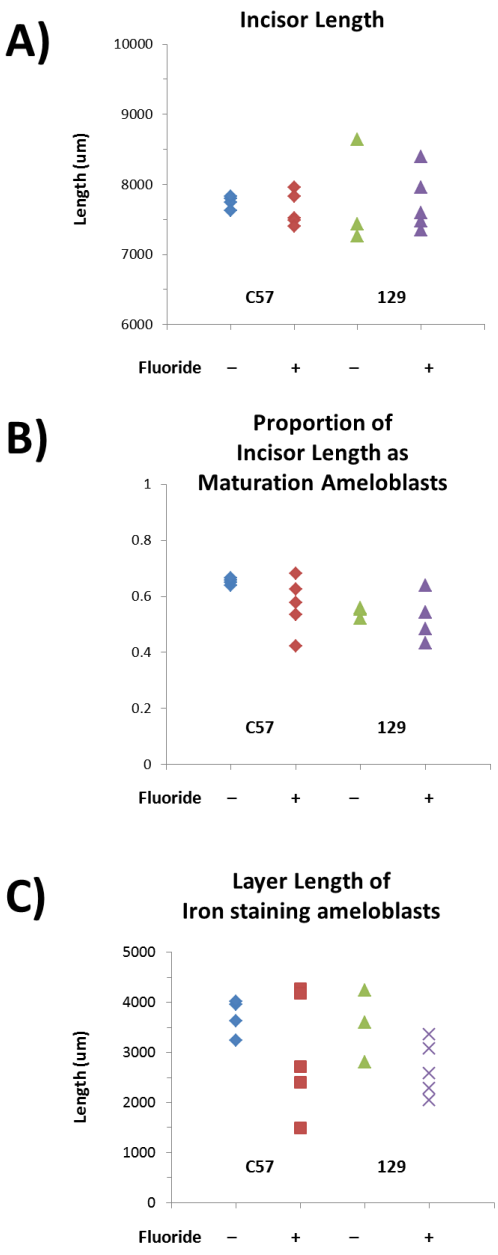

Figure A9 *Distribution of lengths of individual mice when exposed to 0 or 50 ppm F*
(A) Measured lengths of the ameloblast layer in individual C57BL/6 and 129/SvImJ mice given 0 or 50 ppm F.
(B-C) Calculated proportion of the ameloblast layer exhibiting maturation ameloblast phenotype (B) or iron-positive (C) in individual C57BL/6 and 129/SvImJ mice.

A2.4 Discussion

Rodent ameloblasts are well known for the highly accumulated iron in the cytoplasm (Wen and Paine, 2013). As I studied in this section, the ultimate purpose of the iron is to enhance the physical properties of dental enamel. Nevertheless, iron is an important element for many cellular processes, including cellular respiration and DNA repair (Cammack et al., 1990). Therefore, the fluoride induced change in the iron homeostasis would affect cellular function at the maturation stage as well. An unexpected finding in this study was that fluoride exposure was associated with early transition of ameloblasts from maturation to post-maturation. This finding suggests the possibility that the hypomineralized fluorosed enamel phenotype is in part caused by an early dedifferentiation (or terminal differentiation) of ameloblasts at the late maturation stage.

It could be the case that dedifferentiation is caused by a premature change how maturation ameloblasts manage their intracellular iron levels, such as Fe^{2+} chelating fluoride to form iron (II) fluoride (Dodgen and Rollefson, 1949), implying lack of ROS formation and need to store iron in ferritin. Determining if this is the case requires additional studies to other possible forms of iron to determine if fluoride affects iron transport dynamics in maturation ameloblasts.

I examined the length of the ameloblast maturation stage in a dental fluorosis-resistant mouse strain, 129/SvImJ. These mice do not exhibit enamel hypomineralization following exposure to fluoride that is seen in the more dental fluorosis-susceptible C57BL/6 mice. My results suggest that not only fluoride can fluoride induce an early transition from maturation to post-maturation ameloblasts, similar to what is seen in the C57 mice, but also that there is no correlation between incisor pigmentation and length of the maturation ameloblast layer. These findings are providing strong support that incisor pigmentation appears to be a function of the relative hypomineralization of the maturation stage matrix.

Though I did not find a statistical difference to show a fluoride related effect on the length of the maturation stage ameloblasts, it was obvious in comparing the individual data points from both C57 and

129 mice, that fluoride did increase the variability in the length of the maturation stage. I found a published study that showed individual sample responses to 50 ppm F also show variability. Suzuki et al. showed a western blot immunoblotting for KLK4 using maturation enamel matrix of individual rats exposed to 0, 50, and 100 ppm F (Suzuki et al., 2014). Out of 4 individuals exposed to 50 ppm F, 2 individuals showed presence of KLK4. At 100 ppm F, no KLK4 could be detected. If fluoride can reduce the length of the maturation ameloblast layer, then I would expect repeating my studies at 100 ppm F concentration should enable me to consistently find this observation.

Appendix 3
Primers sequences used for all qPCR experiments

All primers are for mouse genome.

Ambn
Forward CTGTTACCAAAGGCCCTGAA
Reverse GCCATTTGTGAAAGGAGAGC

Enam
Forward GCTTTGGCTCCAATTCAAAA
Reverse AGGACTTTCAGTGGGTGT

Mmp20
Forward AGCAAGAGAGGAGATGAAGGTGCT
Reverse AAGGTGGTAGTTGCTCCTGAAGGT

Amel exon6b-d
Forward CAGCAACCAATGATGCCAGTTCCT
Reverse ACTTCTTCCCGCTTGGTCTTGTCT

Amel exon4-6d
Forward AAGTCACATTCTCAGGCTATCAATACT
Reverse ACTTCTTCCCGCTTGGTCTTGTCT

Amtn
Forward CTGTCAACCAGGGAACCACT
Reverse TGTGATGCGGTTTAGCTGAG

Ar
Forward CCCGTCCCAATTGTGTGAAA
Reverse TCCCTGGTACTGTCCAAACG

Ccnd1
Forward TTGTGCATCTACACTGACAAC
Reverse GAAGTGTTCGATGAAATCGT

Eef1a1
Forward CAACATCGTCGTAATCGGACA
Reverse GTCTAAGACCCAGGCGTACTT

Gapdh
Forward TGGCCTTCCGTGTTCCTAC
Reverse GAGTTGCTGTTGAAGTCGCA

Klk4
Forward GGGATACCTGCCTAGTTTCTGG
Reverse AGGTGGTACACGGGGTCATAC

Light chain ferritin (Ftl)
Forward GGGCCTCCTACACCTACCTC
Reverse AGATCCAAGAGGGCCTGATT

Heavy chain ferritin (Fth)
Forward CGAGATGATGTGGCTCTGAA
Reverse GTGCACACTCCATTGCATTC

Ferroportin (Fpn)
Forward TGGATGGGTCCTTACTGTCTGCTAC
Reverse TGCTAATCTGCTCCTGTTTTCTCC

NFkB
Forward AGGCTTCTGGGCCTTATGTG
Reverse TGCTTCTCTCGCCAGGAATAC

Odam
Forward TTGACAGCTTTGTAGGCACA
Reverse GACCTTCTGTTCTGGAGCAA

Runx2
Forward CGGCCCTCCCTGAACTCT
Reverse TGCCTGCCTGGGATCTGTA

Transferrin Receptor (Tfrc)
Forward TCCCGAGGGTTATGTGGC
Reverse GGCGGAAACTGAGTATGATTGA

Wnt10b
Forward TTCTCTCGGGATTTCTTGGATTC
Reverse TGCACTTCCGCTTCAGGTTTTC

Tgfbr2
Forward GGCTTCACTCTGGAAGATGC
Reverse GCTGACACCTGTCACTTGGA

Satb1
Forward TGTGAGTGATCCGAAGGGTC
Reverse GGTTCCTTTCCTAAGGTTGGTTT

Mrpl19
Forward ACGGCTTGCTGCCTTCGCAT
Reverse AGGAACCTTCTCTCGTCTTCCGGG

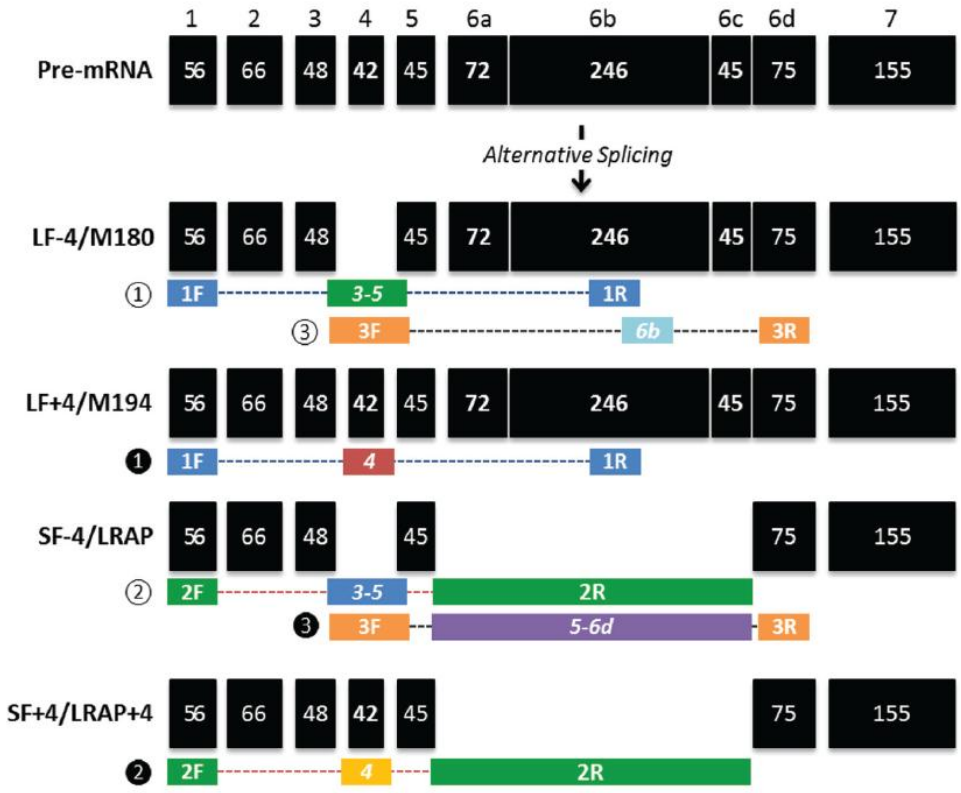

Assay Set	Primer and Probe	Location	Sequence	Amplicon size [bp]	amplicon
①	1F	exon1	CGGATCAAGCATCCCTGAGCTTCA	405	LF-4
	exon3&5	exon3-5 border	FAM-CAACTTAAGCTATGAGGTGCTTACCC-BHQ1		
	1R	exon6b	GGTTGGAGTCATGGAGTGGT		
❶	1F	exon1	CGGATCAAGCATCCCTGAGCTTCA	447	LF+4
	exon4	exon4	FAM-CAGTATTGATAGCCTGAGAATGTGAC-BHQ1		
	1R	exon6b	GGTTGGAGTCATGGAGTGGT		
②	2F	exon1	CGGATCAAGCATCCCTGAGCTTCA	228	SF-4
	exon3&5	exon3-5 border	FAM-CAACTTAAGCTATGAGGTGCTTACCC-BHQ1		
	2R	exon5-6d border	AATGGGGGACAGGGGCGGCTGCCTTATCAT		
❷	2F	exon1	CGGATCAAGCATCCCTGAGCTTCA	270	SF+4
	exon4	exon4	FAM-CAGGCTATCAATACTGACAGGACTGCA-BHQ1		
	2R	exon5-6d border	AATGGGGGACAGGGGCGGCTGCCTTATCAT		
③	3F	exon3-5border	CTTAAGCTATGAGGTGCTTACCC	495	LF-4
	exon6b	exon6b	FAM-ACCATCAGCCAAACATCCCTCCAT-BHQ1		
	3R	exon6d	ACTTCTTCCCGCTTGGTCTTGTCT		
❸	3F	exon3-5border	CTTAAGCTATGAGGTGCTTACCC	132	SF-4
	exon5&6d	exon5-6d border	FAM-AGCATGATAAGGCAGCCGCC-BHQ1		
	3R	exon6d	ACTTCTTCCCGCTTGGTCTTGTCT		

Figure A10 *Quantitative polymerase chain reaction strategy to quantify the expression of amelogenin mRNA splice variants.* Top: Six overlapping primer and probe sets, ①, ❶, ②, ❷, ③, and ❸, were designed to compare the amelogenin mRNA splice variants, including amelogenins containing exon6abc (long form, with exon4 [LF+4] or without exon4 [LF-4]) and amelogenins lacking exon6abc (short form, with exon4 [SF+4] or without exon4 [SF-4]). Bottom: Details of sequences for the primer and probe sets.

Publishing Agreement

It is the policy of the University to encourage the distribution of all theses, dissertations, and manuscripts. Copies of all UCSF theses, dissertations, and manuscripts will be routed to the library via the Graduate Division. The library will make all theses, dissertations, and manuscripts accessible to the public and will preserve these to the best of their abilities, in perpetuity.

I hereby grant permission to the Graduate Division of the University of California, San Francisco to release copies of my thesis, dissertation, or manuscript to the Campus Library to provide access and preservation, in whole or in part, in perpetuity.

2016/09/09

Author Signature | Date (Y/M/D)